

Hypothalamus-sympathetic-liver axis mediates the early phase of stress-induced hyperglycemia in the male mice

Received: 12 March 2024

Accepted: 23 September 2024

Published online: 05 October 2024



Ling Liu^{1,2,3,8}, Zhaohuan Huang^{1,2,8}, Jian Zhang^{1,2,8}, Mengtian Wang^{1,4}, Ting Yue³, Wei Wang¹, Yue Wu¹, Zhi Zhang^{1,3,5}, Wei Xiong^{1,2,6}, Chao Wang^{1,6}, Feng Wu^{2,4}, Cheng Zhan^{1,7}, Guoqiang Bi^{1,2,3} & Ji Liu^{1,2,3,4}✉

Rapid glucose supply is crucial for animal survival during stress response. How the timescale of stress-induced glucose release precisely controlled by hypothalamic corticotropin-releasing hormone (CRH) neurons remains unclear. Here, we show that stress-induced hyperglycemia can be divided into at least two stages in male mice: the first fast stage is mediated by hypothalamus (paraventricular to ventromedial hypothalamus)-sympathetic (raphe pallidus nucleus to intermediolateral nucleus)-liver (HSL) axis activity; the second delayed stage is mediated by adrenal activity. Blocking the activity of HSL axis impairs predatory evoked *flight* responses, indicating that the HSL pathway activity is necessary for stress coping. We further reveal the intracellular signal cascade for CRH signal in the hypothalamus, which is mediated by GABA_A receptor $\beta 3$ subunit phosphorylation at S408/409, results in prevention of GABA_A receptor membrane recruitment. Thus, we uncovered the precise timescale of glucose supply during stress which is mediated by adrenal independent HSL and adrenal dependent pathway respectively.

When facing stressors, the central nervous system initiates a signaling cascade through the hypothalamus-pituitary-adrenal (HPA) and sympathetic-adrenal-medullary (SAM) axes to coordinate the appropriate cellular response with the primary outcome of increasing blood glucose levels¹. Both the HPA and SAM axes are thought to mediate stress-induced hyperglycemia, by releasing hormones from the adrenal, i.e., corticosterone, epinephrine, and norepinephrine, and

secondarily effect on glucose release^{2–6}. However, it usually takes 10–45 min to reach the peak of corticosterone levels in circulation regarding different stressors^{7,8}, which does not fit the *'fight-or-flight'* model because the body needs to mobilize the energy supply immediately after acute stress, such as a predator. While epinephrine mediates a relatively quick release of glucose, yet a couple of minutes to induce blood glucose increase by administrating intravenously^{9–11}.

¹Department of Endocrinology, The First Affiliated Hospital of USTC, National Engineering Laboratory for Brain-inspired Intelligence Technology and Application, School of Information Science and Technology, University of Science and Technology of China, Huangshan Road 443, Hefei 230027, China. ²Institute of Artificial Intelligence, Hefei Comprehensive National Science Center, West WangJiang Road 5089, Hefei 230088, China. ³CAS Key Laboratory of Brain Function and Diseases, Center for Advanced Interdisciplinary Science and Biomedicine of IHM, Division of Life Sciences and Medicine, University of Science and Technology of China, Huangshan Road 443, Hefei 230027, China. ⁴MoE Key Laboratory of Brain-inspired Intelligent Perception and Cognition, University of Science and Technology of China, Huangshan Road 443, Hefei 230027, China. ⁵Department of Anesthesiology and Pain Medicine, The First Affiliated Hospital of USTC, Division of Life Sciences and Medicine, University of Science and Technology of China, LuJiang Road 17, Hefei 230001, China. ⁶Department of Neurology, The First Affiliated Hospital of USTC, Division of Life Sciences and Medicine, Hefei National Research Center for Physical Sciences at the Microscale, University of Science and Technology of China, LuJiang Road 17, Hefei 230001, China. ⁷Department of Hematology, The First Affiliated Hospital of USTC, Division of Life Science and Medicine, University of Science and Technology of China, LuJiang Road 17, Hefei 230001, China. ⁸These authors contributed equally: Ling Liu, Zhaohuan Huang, Jian Zhang. ✉e-mail: Lj1257@ustc.edu.cn

Thus, it is important to understand the timescale of glucose supply and whether there is an alternative pathway that mediates even faster glucose release during stress.

Components of the glucose homeostasis system include humoral and neural signals¹². The humoral signals mediated stress-induced hyperglycemia is relatively clear, which is dependent on adrenal activity^{1,2,5}. Yet how the neural pathway regulates glucose release during stress response remains largely unknown. Corticotropin-releasing hormone (CRH) neurons in the paraventricular nucleus of the hypothalamus (PVN) play a central role in the regulation of HPA axis activity, which stimulates adrenocorticotrophic hormone release and results in the release of corticosteroids from the adrenal gland¹³. The neuropeptide CRH orchestrates neuroendocrine stress signaling via two G protein-coupled receptor subtypes, CRH receptor subtype 1 (CRHR1) and CRH receptor subtype 2 (CRHR2), which are distributed widely in the hypothalamus^{14,15}. The hypothalamus is an important metabolic center for “gut-brain” activity regulation and has been well characterized in terms of its function in glucose metabolism^{2,12,16–19}. However, whether hypothalamic CRH signaling and which CRHR is involved in regulating glucose metabolism remains enigmatic.

In this study, we investigated the time windows for adrenal-dependent and adrenal-independent regulation of stress-induced hyperglycemia. We then applied virus tracing and optogenetic manipulations to reveal the neural pathway initiated from the PVN^{CRH} to the sympathetic nervous system, which is involved in regulating glucose homeostasis during the stress response. Finally, we used electrophysiology to explore the intracellular signaling pathway upon CRH receptor activation in the ventromedial hypothalamus (VMH).

Results

CRH regulated both rapid and delayed glucose releases during acute stress

When facing a stressor, CRH neurons in the PVN are activated, which results in corticosterone release from the adrenal gland. We first asked whether CRH neurons in the PVN regulate glucose levels. To avoid feeding-induced variation of blood glucose, we fasted the testing mice for 12 hours before experiments. First, we expressed excitatory DREADDs, hM₃Dq, in the PVN by injecting Cre-recombinase dependent AAV-(double floxed inverted open reading frame) DIO-hM₃Dq into *Crh-Cre* mice (Fig. 1a). Administration of the DREADD ligand clozapine-N-oxide (CNO) significantly increased firing rate of CRH neurons (Fig. 1a), and c-fos expression in CRH neurons (Supplementary Fig. 1a–c). Intraperitoneally injecting CNO resulted in an increase in blood glucose levels in the experimental group compared to the control group, which expressed AAV-DIO-mCherry in CRH neurons (Fig. 1b). To further confirm the results, we used an optogenetic approach by expressing AAV-DIO-ChR2-GFP into the PVN region of *Crh-Cre* transgenic mice, into which optical fibers had been implanted (bilaterally) in the PVN region (Fig. 1c, Supplementary Fig. 1d). As expected, in vitro electrophysiological recordings in brain slices showed increased activity of PVN^{CRH} neurons when exposed to blue light (Fig. 1c, Supplementary Fig. 1e). Consistent with the chemogenetic data, optical stimulation of CRH neurons caused significant increases in blood glucose levels, and corticosterone levels as well (Fig. 1d, Supplementary Fig. 1f, g), suggesting that activation of PVN^{CRH} neurons was indeed able to regulate glucose levels.

If PVN^{CRH} is involved in the regulation of glucose levels, the next question is whether CRH is necessary to regulate glucose release during stress response. Physical stressors (e.g., lipopolysaccharide, LPS, injection, footshock, and tail clip) are commonly used in mouse studies. To investigate the rapid and slow time windows of glucose response during stress, we define the timepoint immediately after stress as “fast glucose” and the timepoint of 30 min after stress as “delayed glucose”. Considering that LPS did not induce hyperglycemia within a rapid time window (Supplementary Fig. 1h, i), we used a

footshock stressor to determine whether stress-induced glucose levels are dependent on CRH activation. To do so, we expressed AAV-DIO-eNpHR-GFP into the PVN region of *Crh-Cre* mice, and implanted bilateral optic fibers at the same position (Fig. 1e, Supplementary Fig. 1j). When exposed to 589 nm light, CRH neuronal activity was decreased as expected (Fig. 1f). Suppression of CRH neuronal activity inhibited footshock stress-induced hyperglycemia for both fast glucose and delay glucose when compared to the control group, which expressed AAV-DIO-EGFP in the CRH neurons (Fig. 1g). Our results showed that PVN^{CRH} activation is necessary for regulating glucose levels at both early and later stages of acute stress.

CRH-initiated activation of the HPA axis is dependent on adrenal activity. To test whether adrenal activity is necessary for glucose release during acute stress, we performed adrenalectomy (ADX) to remove the possible adrenal hormones release (Fig. 1h). As expected, corticosterone (CORT) levels were not changed during footshock stress in the ADX mice (Supplementary Fig. 1k, l). Footshock stress increased fast blood glucose levels for both sham and ADX groups when compared with baseline (Fig. 1i). Previous studies indicated that ADX may affect stress-induced glucose levels^{20,21}, here we showed that ADX did suppress glucose rising for delayed glucose (Fig. 1i), suggesting that adrenal activity is required for stress-induced glucose at later phase. Interestingly, when compared with the control group, which were without stress, the early phase of glucose levels was higher in both sham and ADX groups (Fig. 1i), suggesting that adrenal activity is not necessary for fast glucose release.

Considering that many adrenal hormones will be release during stress, we used corticosterone receptor-specific antagonist, CORT108297, and mifepristone to specifically block the reaction of CORT during stress. Again, we found that CORT108297 and mifepristone can only suppress stress-induced delay glucose response but not fast glucose levels (Fig. 1j, k, Supplementary Fig. 1m, n). Thus, our data suggested that beyond the HPA axis-dependent glucose response, there may be an alternative pathway that mediates rapid glucose release during the stress response independent of adrenal activity.

PVN^{CRH}-VMH projection is required for rapid glucose release during stress

To explore the possible downstream targets of CRH neurons, we chemogenetically activated PVN^{CRH} neurons and performed immunostaining for c-Fos, a neuronal activity marker (Fig. 2a). As showed above, stimulation of PVN^{CRH} neurons significantly increased c-Fos-positive cell numbers in PVN^{CRH} neurons (Supplementary Fig. 1a–c). Interestingly, we also found increased c-Fos expression in the VMH (Fig. 2b, c). Steroidogenic factor 1 (SF-1) is an orphan nuclear hormone receptor that is expressed specifically in the VMH. To further test whether VMH neurons were involved in the stress response, we expressed Cre-dependent GCaMP6 in VMH^{SF-1} neurons by the stress response, we expressed Cre-dependent GCaMP6 in VMH^{SF-1} neurons by injecting AAV-DIO-GCaMP6 into *Sf-1-Cre* mice (Fig. 2d). In response to acute physical stress, including footshock, water spray, and tail clip, we found overall >20% changes in bulk Ca²⁺ signals (indicated by $\Delta F/F$) (Fig. 2e, Supplementary Fig. 2a–c). This suggests that VMH^{SF-1} neurons are indeed involved in the stress response.

If VMH neurons respond to both stress and stimulation of PVN^{CRH} neurons, we asked whether VMH neurons receive afferents from PVN^{CRH} neurons. To test this hypothesis, we first injected the anterograde tracing virus AAV-DIO-synaptophysin-mGFP into the PVN of *Crh-Cre* mice, and densely labeled terminals were found in the VMH region (Fig. 2f, g). To test whether PVN^{CRH} formed monosynaptic connections with VMH neurons, we expressed AAV-DIO-ChR2 in the CRH neurons. When exposure to blue light, time-locked post synaptic excitatory currents were found in VMH neurons, which can be blocked by pre-synaptic blocker TTX and recovered by TTX + 4-AP, indicating a monosynaptic connection between PVN^{CRH}

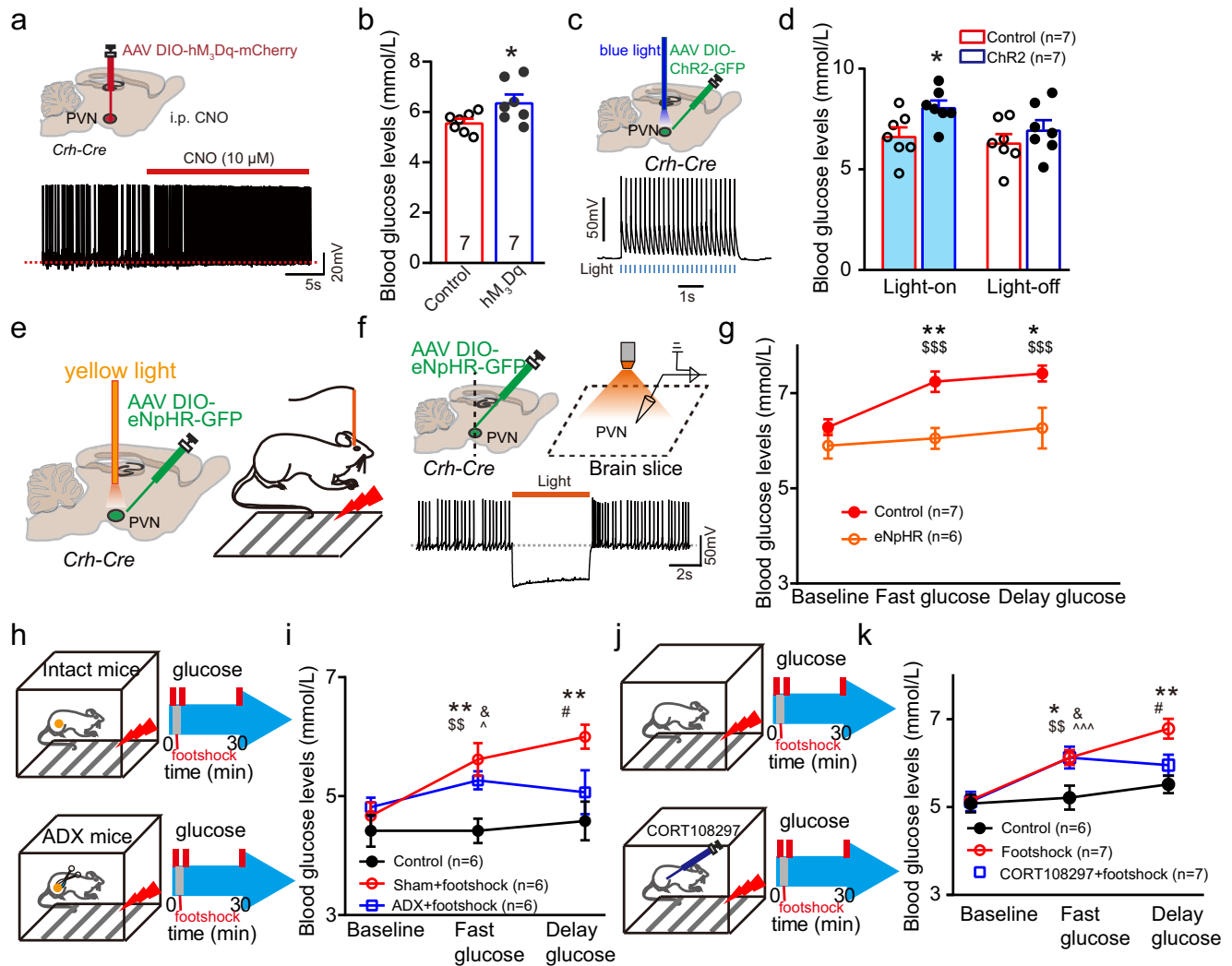


Fig. 1 | HPA axis mediated hyperglycemia. **a** Experimental paradigm for chemo-genetic activation of PVN^{CRH} neurons in *Crh-Cre* mice (top). The firing rate of PVN^{CRH} neurons increased after treatment with 10 μ M CNO (down). **b** Activation of PVN^{CRH} neurons significantly increased glucose levels ($n = 7$ per group). * $p = 0.039$. **c** Experimental paradigm for optogenetic stimulation of PVN^{CRH} in *Crh-Cre* mice (top). Example trace showing the firing rate of PVN^{CRH} neurons in response to blue light exposure (down). **d** Photo-stimulation of CRH neurons increased glucose levels compared to control (injected with AAV-DIO-GFP, $n = 7$ per group). * $p = 0.022$. **e** Experimental paradigm for optogenetic inhibition of PVN^{CRH} in *Crh-Cre* mice during footshock stress. **f** Example trace showing the firing rate of CRH neurons in response to yellow light exposure. **g** Inhibition of PVN^{CRH} neurons significantly suppressed stress-induced blood glucose ($p = 0.015$, $n = 7$ for control and $n = 6$ for eNpHR). Post-hoc test: control vs eNpHR, ** $p = 0.003$ (fast), * $p = 0.022$ (delay); for control: \$\$\$ $p < 0.001$, compared to baseline. **h** Experimental paradigm for footshock stress in intact and adrenalectomized (ADX) mice. **i** Footshock stress

increased blood glucose levels in both fast ($p = 0.004$) and delay stages ($p = 0.016$) ($n = 6$ per group). Post-hoc test showed increased fast glucose levels in both sham (** $p = 0.001$) and ADX (& $p = 0.014$) group when compared to control group (without stress). While sham group showed higher delay glucose than control (** $p = 0.005$) and ADX (# $p = 0.048$) group. When compared to baseline, \$\$\$ $p = 0.008$ for sham and ^ $p = 0.018$ for ADX group. **j** Experimental paradigm for footshock stress with/out CORT108297 injection. **k** Footshock stress increased glucose levels in both fast ($p = 0.02$) and delay stages ($p = 0.003$) ($n = 6$ for control, $n = 7$ for other two groups). Post-hoc test: footshock vs control, * $p = 0.014$ (fast), ** $p = 0.001$ (delay); CORT108297+footshock vs control, & $p = 0.014$ (fast); footshock vs CORT108297+footshock, # $p = 0.016$ (delay). When compared to baseline, \$\$\$ $p = 0.002$ (Footshock) and ^ $p < 0.001$ (CORT108297+footshock). Multi-time point data were analyzed by two-way repeated-measures ANOVA with LSD post hoc comparison, otherwise use two-sided t test. All data shown as means \pm SEM. Source data are provided as a Source Data file.

and VMH neurons (Fig. 2h, i). To further confirm this pathway, we used a modified rabies virus SAD Δ G-EGFP (EnvA- SAD Δ G-EGFP) in combination with Cre-dependent AAV-TVA (receptor for the avian sarcoma leucosis virus glycoprotein EnvA; AAV-DIO-mCherry-TVA) and RG (rabies envelope glycoprotein; AAV-DIO-RV-G) injected into *Sf-1-Cre:Crh-Flpo* double transgenic mice. Three weeks prior to SAD Δ G-EGFP injection, the Flpo-dependent expression of mCherry AAV (AAV-fDIO-mCherry) was injected into the PVN to label CRH-expressing neurons (Fig. 2j). Flpo-dependent expression of mCherry nicely colocalized with CRH antibody staining (Supplementary Fig. 2d–f), indicating the virus specifically expressed in the CRH neurons. GFP-positive cells projecting to VMH^{SF-1} neurons were

found in the PVN area, and ~42% of them were also mCherry positive, indicating the expression of CRH-Flpo recombinase (Fig. 2k, l). Thus, we provided strong evidence to show the structural connection between PVN^{CRH} and VMH^{SF-1} neurons.

If VMH^{SF-1} neurons receive projections from the PVN^{CRH}, we next asked whether the PVN^{CRH}–VMH^{SF-1} pathway mediates glucose levels. To do so, we implanted optical fibers (bilaterally) in the VMH region of *Crh-Cre:Ai32* mice (expressing ChR2 in CRH neurons) (Fig. 2m, Supplementary Fig. 2g). Optical stimulation of CRH nerve terminals in the VMH caused a significant increase in blood glucose (Fig. 2n). This result supports that optogenetic activation of PVN^{CRH} to VMH projection functions directly in increasing blood glucose levels.

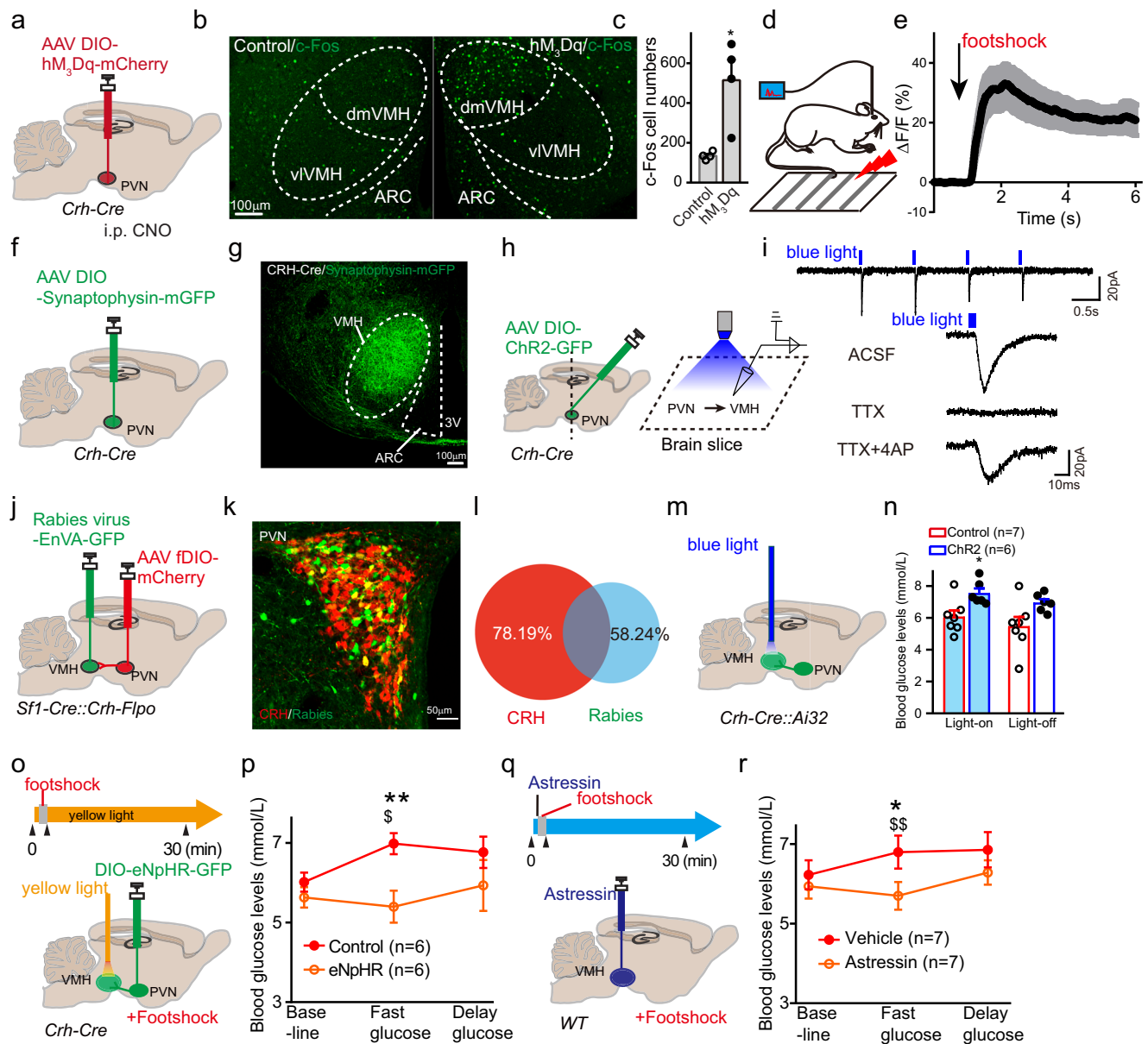


Fig. 2 | PVN^{CRH}-VMH^{SF1} projection regulates stress-induced hyperglycemia.

a Paradigm of chemogenetic activation of PVN^{CRH} neurons. **b, c** Representative image (**b**) and quantification (**c**) of c-Fos positive cell numbers in the VMH of Control and hM3Dq expression mice. $n = 4$ mice per group. $*p = 0.01$. **d** Paradigm of fiber-photometry recording of VMH^{SF1} neurons during footshock stress. **e** Approximately 30% Ca^{2+} signal change was observed in SF-1 neurons in response to footshock stimulation. $n = 6$ mice. **f, g** Paradigm of (f) anterograde tracing virus injection and typical image (**g**) of mGFP expression in the VMH originating from CRH afferents. **h** Paradigm of photo-stimulation of PVN \rightarrow VMH in *Crh-Cre* mice. **i** Example traces for light-evoked time-locked EPSC in the VMH neurons. **j, k** Paradigm of pseudorabies virus mediated retrograde tracing (**j**) and representative image (**k**). **l** Approximately, 42% SF-1 projecting cell are CRH positive, while approximately 22% CRH neurons are projecting SF-1, $n = 4$ mice. **m** Paradigm

of photo-stimulation of PVN^{CRH} \rightarrow VMH. **n** Glucose level is significantly increased after exposure to blue light in ChR2 group ($n = 6$) compared to control group ($n = 7$). $*p = 0.015$. **o** Schematic of photo-inhibition of PVN^{CRH} \rightarrow VMH during footshock. **p** Inhibition of PVN^{CRH} \rightarrow VMH suppressed stress-induced blood glucose in fast stage ($**p = 0.008$, control vs eNpHR, $n = 6$ per group). $\$p = 0.017$, when compared to baseline in control group. **q** Paradigm of microinjection of CRH receptor antagonist Astressin in the VMH. **r** Administration of Astressin blocked glucose increases of fast glucose response ($*p = 0.043$, Vehicle vs Astressin, $n = 7$ per group). $\$p = 0.004$, when compared to baseline in vehicle group. Multi-time point data were analyzed by two-way repeated-measures ANOVA with LSD post hoc comparison, otherwise use two-sided t test. All data shown as means \pm SEM. Source data are provided as a Source Data file.

Stimulation of CRH terminal in the VMH did not cause any changes of CORT levels (Supplementary Fig. 2h), suggesting that the increased glucose levels by stimulating of PVN-VMH was not mediated by CORT. To investigate whether the PVN^{CRH} to VMH neural circuit is necessary to mediate stress-induced glucose levels, we expressed light-sensitive natronomonas halorhodopsin (NpHR) in CRH neurons by injecting AAV-DIO-eNpHR-GFP into the PVN of *Crh-Cre* mice (Fig. 2o, Supplementary Fig. 2i). As expected, footshock-induced an increase

in blood glucose levels in the control group, which expressed AAV-DIO-GFP in the PVN (Fig. 2p). Optogenetic inhibition of the PVN^{CRH} to VMH blocked the footshock-induced hyperglycemic for fast glucose, but not for delay glucose (Fig. 2p). Photo-inhibition of PVN^{CRH} to VMH pathway didn't effect on CORT levels (Supplementary Fig. 2j), indicating the suppression of fast glucose level was not mediated by CORT. Inhibition of PVN^{CRH}-VMH under no-stress condition did not change glucose levels (Supplementary Fig. 2k, l). Interestingly, when

we infused the nonselective CRH receptor antagonist Astressin into the VMH via a bilateral guide cannula (Fig. 2q, Supplementary Fig. 2m), the footshock-induced increase in fast glucose levels was significantly suppressed, but not in delay glucose levels, when compared to the vehicle group (Fig. 2r). These results indicated that the PVN^{CRH} to VMH projection is necessary to regulate rapid glucose release during stress, which is likely mediated by CRH receptor activation in the VMH.

CRH-initiated rapid glucose release is mediated by VMH^{CRHR2} during stress

Above, we provide evidence that CRH receptor activation is necessary to regulate stress-induced hyperglycemia. Both CRHR1 and CRHR2 are widely distributed in the brain, while the majority of the CRH receptor subtype in the VMH is CRHR2¹⁵. To study whether CRHR2 is responsible for glucose modulation during the stress response, we infused different CRH receptor antagonists into the VMH and measured the blood glucose changes (Fig. 3a, Supplementary Fig. 3a, b). Application of the CRHR1 antagonist R121919 showed a modest change in blood glucose levels (Supplementary Fig. 3c), while the CRHR2 antagonist Astressin2B blocked the fast glucose increase (Fig. 3b) when compared to the vehicle group during footshock stress. Similarly, Astressin2B blocked the fast glucose elevation but not in the delay phase when facing other stressors, including water spray, tail clamp, and looming (Supplementary Fig. 3d–g), which confirmed that CRH signal-mediated hyperglycemia during the stress response is mainly mediated by activation of CRHR2 in the VMH. When we labeled VMH neurons by injecting AAV-DIO-GFP into *Sf-1-Cre* mice and probed *Crhr2* mRNA with specific antisense oligonucleotides, we found abundant *Crhr2* mRNA expressed in the dorsomedial VMH (Fig. 3c, d).

To further confirm that CRHR2 activation is necessary for stress-induced hyperglycemia, we crossed *Sf-1-Cre* mice with *Crhr1^{fllox}* and *Crhr2^{fllox}* mice to generate *Sf-1^{Cre}Crhr1^{-/-}* and *Sf-1^{Cre}Crhr2^{-/-}* mice, respectively (Fig. 3e and Supplementary Fig. 3i). RNAScope results showed that *Crhr2* mRNA expression was completely diminished in SF-1-positive cells (Fig. 3f), but not in the littermate (control) mice (Supplementary Fig. 3h). Consistently, *Crhr2* knockout mice showed blunted fast blood glucose increases in response to footshock water spray, tail clamp and looming when compared to the control animals (Fig. 3g, h, Supplementary Fig. 4a–d). While *Crhr2* knockout mice with ADX completely blocked footshock stress-induced hyperglycemia (Fig. 3h). As a control experiment, we did not observe a significant change in the *Crhr1* knockout group (Supplementary Fig. 3j). This result indicated that CRHR2 activation in the VMH is necessary to regulate stress-induced hyperglycemia, at least at the early stage of the stress response.

To further investigate whether VMH^{CRHR2} and HPA axis activity mediate different stages of glucose release during stress, we injected the CRHR2 antagonist Astressin2B into the VMH following bilateral removal of the adrenal glands from WT mice (Fig. 3i, Supplementary Fig. 4e, f). Consistent with Fig. 1j, an increase in fast blood glucose was observed post-footshock stimulation in adrenalectomized mice, which was completely diminished by infusion of Astressin2B through a bilateral guide cannula in the VMH (Fig. 3j). These data suggested that the VMH CRH signal responds to the early stage of stress-induced hyperglycemia, while the release of adrenal hormones responds to the delayed stage of stress. To further confirm our results, we injected CORT receptors antagonist CORT108297 and mifepristone, combining with VMH infusion of Astressin2B (Fig. 3k, Supplementary Fig. 4g). When compared to vehicle group, CORT108297 and mifepristone blocked delay glucose levels after stress, but not for the fast glucose levels (Fig. 3l, Supplementary Fig. 4h). While CORT108297/mifepristone+Astressin2B completely blocked stress-induced hyperglycemia (Fig. 3l, Supplementary Fig. 4h). Thus, we provided the evidence that activation of CRHR2 in the VMH is necessary for fast glucose response during acute stress.

CRH suppresses inhibitory synaptic transmission via the $\beta 3$ GABA_A receptor subunit in the VMH

The above results showed that CRH receptor activation in the VMH is required for regulating the stress-induced glucose response. The next question is how the CRH regulates VMH neuronal activity. To address this question, we injected AAV-DIO-GFP to label VMH neurons in *Sf-1-Cre* mice and characterized spontaneous action potential firing properties with the current-clamp recording (Fig. 4a). An increased action potential firing rate was observed with the application of 100 nM CRH peptide (Fig. 4b, c), indicating that CRH can excite VMH neurons. As expected, CRH-induced increases in the firing rate were completely diminished when recording action potentials in *Sf-1^{Cre}Crhr2^{-/-}* mice (Fig. 4d, e) but not in *Sf-1^{Cre}Crhr1^{-/-}* mice (Supplementary Fig. 5a–c), again indicating that the CRH-induced excitatory effect is mediated by CRHR2.

We showed that CRH excites VMH neuronal activity. However, whether this excitatory effect is mediated by synaptic transmission is unknown. To answer this question, we performed voltage clamp to record the postsynaptic currents in VMH^{SF-1} neurons. Application of CRH did not affect spontaneous excitatory postsynaptic currents (sEPSCs) (Supplementary Fig. 5d–f). While perfusion with GABA_A receptor antagonist PTX blocked CRH effect on action potential firing (Fig. 4f, g), indicating inhibitory currents may mediate CRH's effect on VMH neuronal activity. Indeed, CRH significantly decreased the amplitude and frequency of spontaneous inhibitory postsynaptic currents (sIPSCs) (Fig. 4h–j). Again, knocking out *Crhr2* expression in VMH^{SF-1} neurons completely diminished the CRH-induced inhibition of sIPSC amplitude and frequency (Fig. 4k–m), while knocking out *Crhr1* expression did not affect the inhibitory effect of CRH on sIPSCs in VMH^{SF-1} neurons (Supplementary Fig. 5g–i). It suggested that CRHR2 activation suppressed inhibitory tone in SF-1 neurons.

We further determined whether the inhibitory effect of CRH on IPSCs is a pre- or postsynaptic effect by blocking pre-synaptic effects with perfusion of tetrodotoxin (TTX). The amplitude of miniature IPSCs (mIPSCs) was significantly suppressed by CRH (Fig. 5a, b), while no significant difference was found in miniature EPSCs (mEPSC) amplitude (Supplementary Fig. 6a, b). The frequencies of both mIPSCs and mEPSCs were not changed by the application of CRH (Supplementary Fig. 6c, d), suggesting that a postsynaptic inhibitory tone is selectively targeted by CRH signaling within the VMH. To exclude possible pre-synaptic effects, we analyzed the paired-pulse ratio (PPR) and found no effect on PPR before and after application of CRH (Fig. 5c–e), suggesting that a pre-synaptic mechanism is unlikely to mediate CRH's effect on IPSCs. Finally, we performed evoked IPSC (eIPSC) recording in VMH^{SF-1} neurons by local electric stimulation in the absence or presence of CRH. We found dramatic decreases in amplitude (Fig. 5f, g), which provides strong evidence that CRH suppresses inhibitory synaptic transmission postsynaptically, likely by attenuating the trafficking of GABA_A receptors (GABA_ARs) to the membrane^{22,23}.

If our interpretation that CRH signaling attenuates GABA_AR trafficking is correct, we should be able to directly examine how changes in signaling cascades downstream of CRH receptor activation affect GABA_AR trafficking to the plasma membrane. Most GABA_A receptors are composed of 2α , 2β and 1γ subunits²⁴. To visualize the cell surface dynamics of GABA_ARs, we expressed pHluorin (a pH-sensitive GFP variant)-tagged GABA_AR subunits ($\beta 3$ and $\gamma 2$) together with CRHR2 in the N2a cell line to measure receptor mobility in real time²³. We found a decrease in $\beta 3$ GABA_AR subunits (up to 10% change, presented by $\Delta F/F$) in response to CRH (Fig. 5h, i), while no significant change was found in $\gamma 2$ subunit-expressing cells (Supplementary Fig. 6e).

This result suggested that the $\beta 3$ -containing GABA_AR subunit is selectively targeted by the CRH intracellular signaling pathway. Previous studies have indicated that the membrane trafficking of GABA_AR subunits is likely mediated by phosphorylation of the intracellular

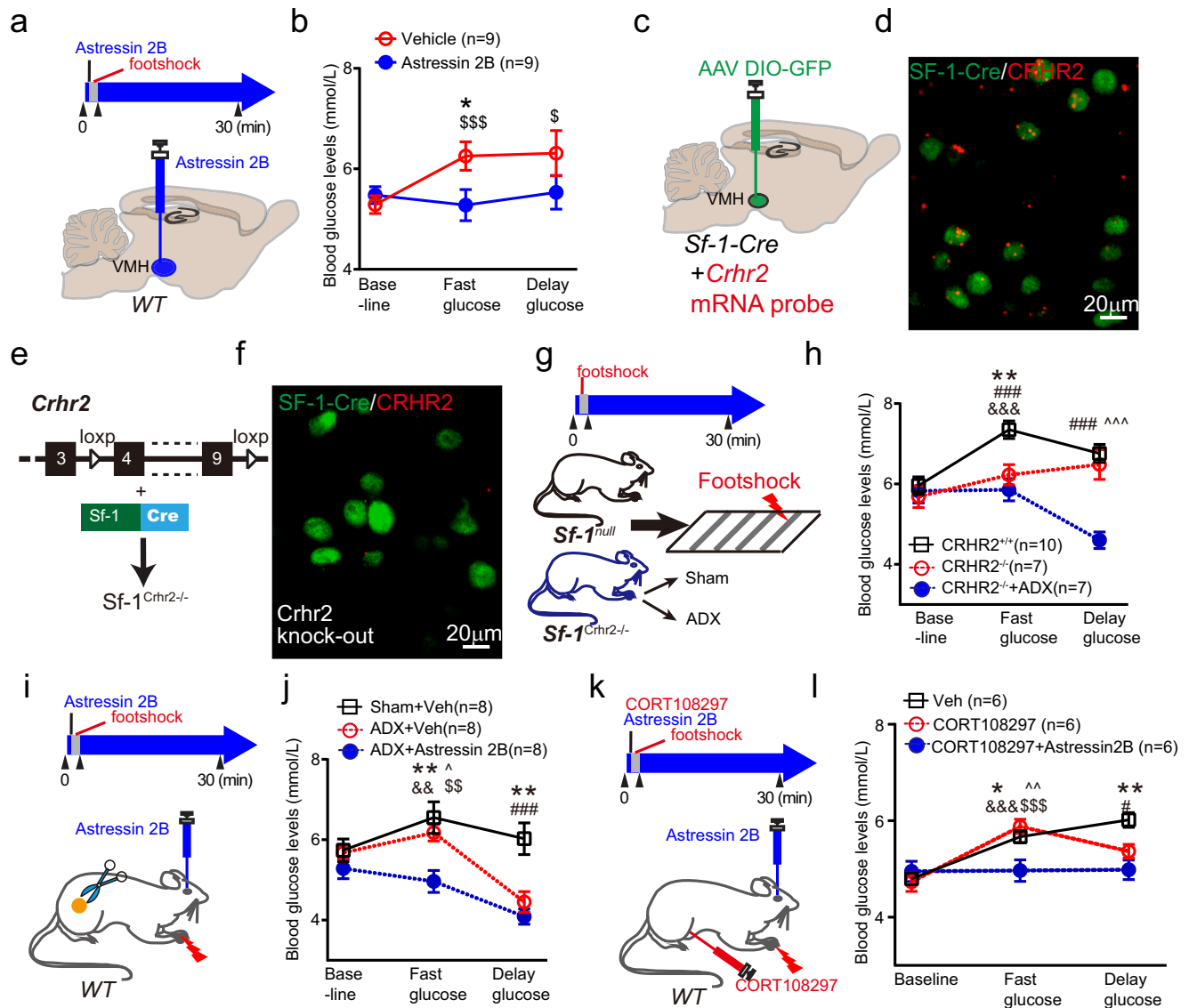


Fig. 3 | CRH receptor2 activation in the VMH is necessary to regulate stress-induced hyperglycemia. **a** Paradigm of microinjection of CRHR2 antagonist Astressin2B in the VMH. **b** Administration of Astressin2B, blocked footshock induced fast glucose increases, $*p = 0.033$, $n = 9$ per group; while for vehicle group, $***p < 0.001$, $p = 0.032$, compared to baseline. **c** Schematic of in situ to detect CRHR2 expression in SF-1 neurons. **d** *Crhr2* mRNA (Red) colocalized with SF-1 neurons (GFP). **e** Paradigm for generating SF-1 neurons selective *Crhr2* knock-out mice. **f** Representative image showed that *Crhr2* mRNA expression was completely knock-out in the SF-1 neurons. **g** Schematic of stress stimulation in *Crhr2* knock-out and ADX groups. **h** Footshock stress-induced glucose levels was different in the three groups ($p = 0.003$). For fast glucose: $**p = 0.004$, $CRHR2^{+/+}$ ($n = 10$) vs $CRHR2^{-/-}$ ($n = 7$); $###p < 0.001$, $CRHR2^{+/+}$ vs $CRHR2^{-/-}$ + ADX ($n = 7$); $\&\&p < 0.001$, fast-stage vs baseline in $CRHR2^{+/+}$ group. For delay glucose, both of two intact groups were higher than ADX group ($###p < 0.001$, $CRHR2^{+/+}$ vs $CRHR2^{-/-}$ + ADX; $^^p < 0.001$, $CRHR2^{-/-}$ vs $CRHR2^{-/-}$ + ADX). **i** Schematic of adrenalectomy and CRHR2 antagonist Astressin2B infusion in VMH. **j** Footshock stress-induced glucose

levels was different in the three groups ($p = 0.003$), $n = 8$ per group. For fast glucose: $**p = 0.001$, sham+Veh vs ADX+Astressin2B; $*p = 0.01$, ADX+Veh vs ADX+Astressin2B; fast-stage vs baseline, $\&\&p = 0.002$ and $$$$p = 0.007$ for sham+Veh and ADX+Veh groups respectively. For delay glucose, sham+Veh was higher than both ADX+Veh ($**p = 0.001$) and ADX+Astressin2B group ($###p < 0.001$). **k** Schematic of CORT108297 injection and Astressin2B infusion in VMH. **l** Footshock stress-induced glucose levels was different in the three groups ($p = 0.039$), $n = 6$ per group. For fast glucose: $*p = 0.011$, Veh vs CORT108297+Astressin2B; $^{\wedge}p = 0.002$, CORT108297 vs CORT108297+Astressin2B; fast-stage vs baseline, $\&\&\&p < 0.001$ and $$$$p < 0.001$ for Veh and CORT108297 groups respectively. For delay glucose, Veh was higher than both CORT108297 and CORT108297+Astressin2B group ($\#p = 0.015$ and $**p = 0.001$, respectively). Multi-time point data were analyzed by two-way repeated-measures ANOVA with LSD post hoc comparison, otherwise use two-sided t test. All data shown as means \pm SEM. Source data are provided as a Source Data file.

domain, specifically, the Ser408/409 phosphorylation site for $\beta 3$ subunits²². Since the phosphorylation of GABA_AR was too low to detect either in vivo or in vitro, we again used N2a cells to enrich $\beta 3$ GABA_AR subunits by first immunoprecipitating (IP) utilizing a pH-sensitive form of GFP tagging and performing western blotting using phosphorylation site-specific antibodies. Remarkably, we found that phosphorylation of S408/409 was drastically increased after CRH treatment (Fig. 5j, k). These data strongly suggested that the Ser408/409

phosphorylation site on the $\beta 3$ GABA_AR subunit is a specific target of CRH signaling in the VMH. If suppression of GABA_AR membrane recruitment mediated CRH's effect on glucose levels, we should be able to mimic this effect by blocking GABA_AR in VMH. To test this, we infused GABA_AR antagonist bicuculline into the VMH via a guide cannula (Fig. 5l). We found an increase in blood glucose levels after bicuculline administration, which suggested that VMH CRH effects on glucose regulation were mediated by GABA_A receptors (Fig. 5m).

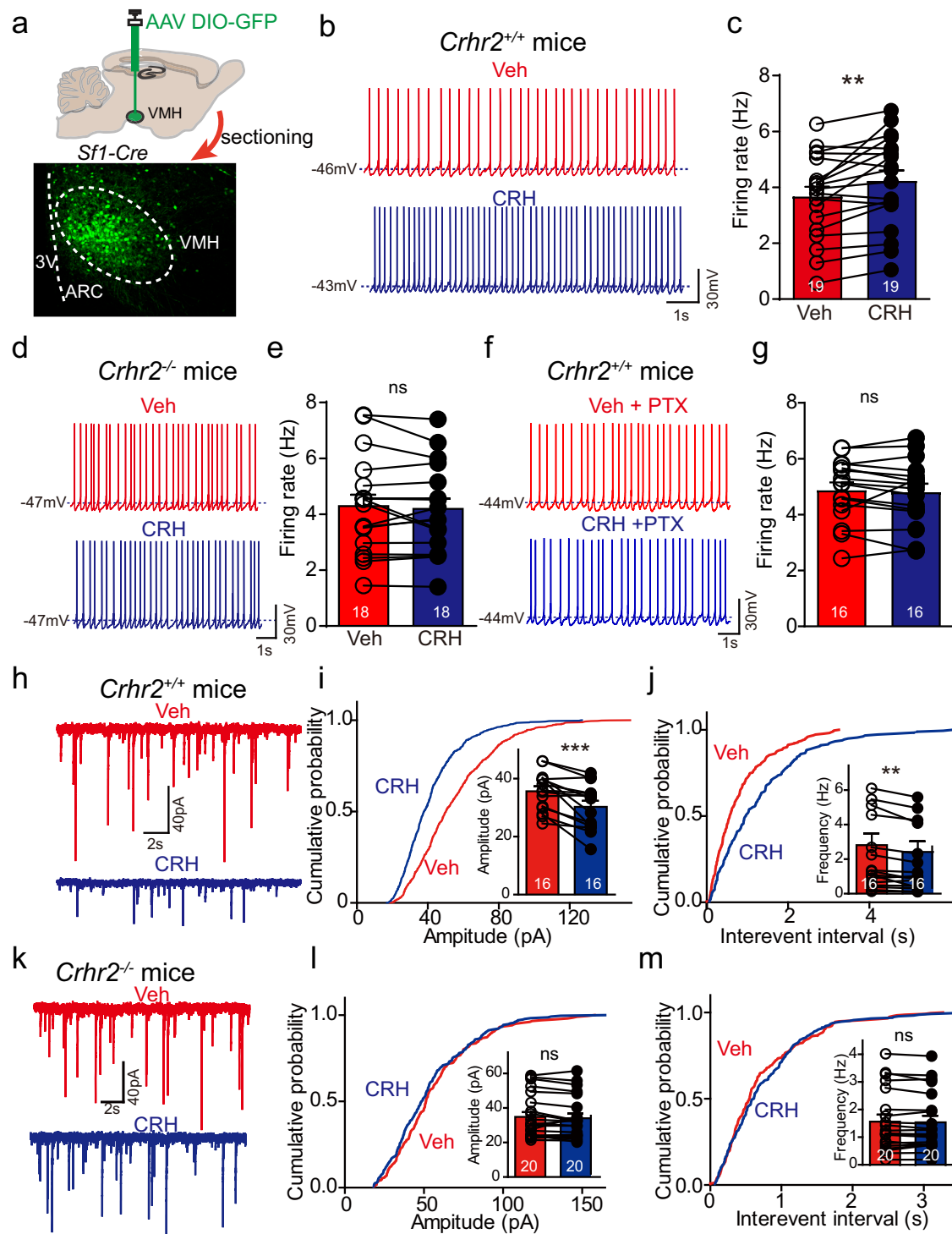


Fig. 4 | Suppress of inhibitory currents mediates CRH excitatory effect in VMH.

a Schematic of the investigation of CRH effects on SF-1 neuronal activity in VMH. **b** Representative trace for recording I-clamp from SF-1 neurons during perfusion with 100 nM CRH in *Sf1-Cre* mice. **c** Firing rate is significantly increased after 100 nM CRH treatment. $n = 19/5$, cells/animals. $p = 0.003$. **d** Representative trace for recording I-clamp from SF-1 neurons during perfusion with 100 nM CRH in *Sf1^{Crhr2-/-}* mice. **e** The excitatory effect induced by CRH can be completely diminished by knock-out *Crhr2* expression in SF-1 neurons. $n = 18/5$, cells/animals. $p = 0.361$. **f** Representative trace for recording I-clamp from SF-1 neurons during perfusion with 100 nM CRH plus GABA_A receptor antagonist PTX in *Sf1-Cre* mice. **g** The excitatory effect induced by CRH can be completely diminished by PTX in SF-1 neurons. $n = 16/4$, cells/animals. $p = 0.558$. **h** Representative traces of sIPSCs in VMH^{SF-1} neurons before and after the application of CRH in *Sf1-Cre* mice.

i Cumulative amplitude probability plots of sIPSCs in typical VMH^{SF-1} neurons before and after CRH application. Inset in **i**: pooled data. $n = 16/4$, cells/animals; $***p < 0.001$, for sIPSCs amplitude. **j** Cumulative frequency probability plots of sIPSCs in typical VMH^{SF-1} neurons before and after CRH application. Inset in **j**: pooled data. $n = 16/4$, cells/animals; $p = 0.008$, for sIPSCs frequency. **k** Representative traces of sIPSCs in VMH^{SF-1} neurons before and after the application of CRH in *Sf1^{Crhr2-/-}* mice. The CRH induced inhibition of amplitude (**l**) and frequency (**m**) on sIPSCs can be completely diminished by knock-out *Crhr2* expression in SF-1 neurons. Inset in **l**: pooled data. $n = 20/5$, cells/animals; $p = 0.446$. Inset in **m**: pooled data. $n = 20/5$, cells/animals; $p = 0.301$. Two-sided paired *t* test in (**c**, **e**, **g**, **i**, **j**, **l**, **m**). All data are shown as means \pm SEM. $*p < 0.05$, $**p < 0.01$, $***p < 0.001$; ns, not significant. Source data are provided as a Source Data file.

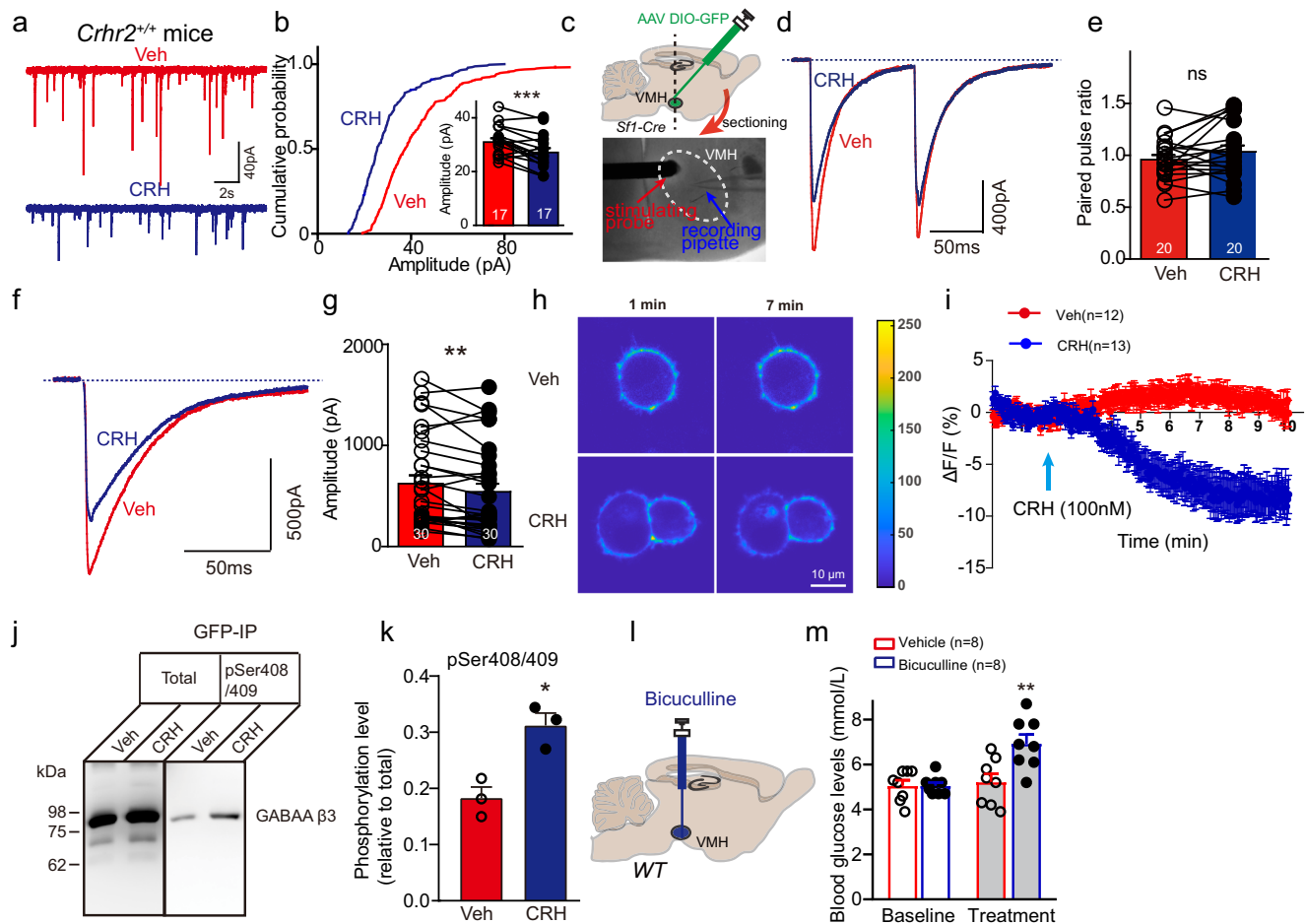


Fig. 5 | $\beta 3$ GABA_A receptor subunit membrane trafficking mediates CRH excitatory effect in VMH. **a** Representative traces of mIPSCs in VMH^{SF1} neurons before and after the application of CRH in *Sf1-Cre* mice. **b** Cumulative amplitude probability plots of mIPSCs in typical VMH^{SF1} neurons before and after CRH application. Inset in b: pooled data. $n = 17/4$, cells/animals; *** $p < 0.001$, for mIPSC amplitude. **c** Schematic of evoked IPSCs recording from SF-1 neurons in *Sf1-Cre* mice. **d** Representative traces of pair pulse ratio in the presence of CNQX in VMH^{SF1} neurons. **e** CRH treatment did not effect on pair pulse ratio, indicating unlikely a pre-synaptic effect, $n = 20/5$, cells/animals; $p = 0.138$. **f** Representative traces of evoked IPSCs (eIPSCs) in the presence of CNQX in VMH^{SF1} neurons. **g** CRH treatment significantly decreased eIPSC amplitudes, $n = 30/6$, cells/animals; $p = 0.005$. **h** Representative image showed $\beta 3$ GABA_A receptor subunit membrane trafficking in response to vehicle and CRH treatment, respectively. **i** Overall, CRH treatment

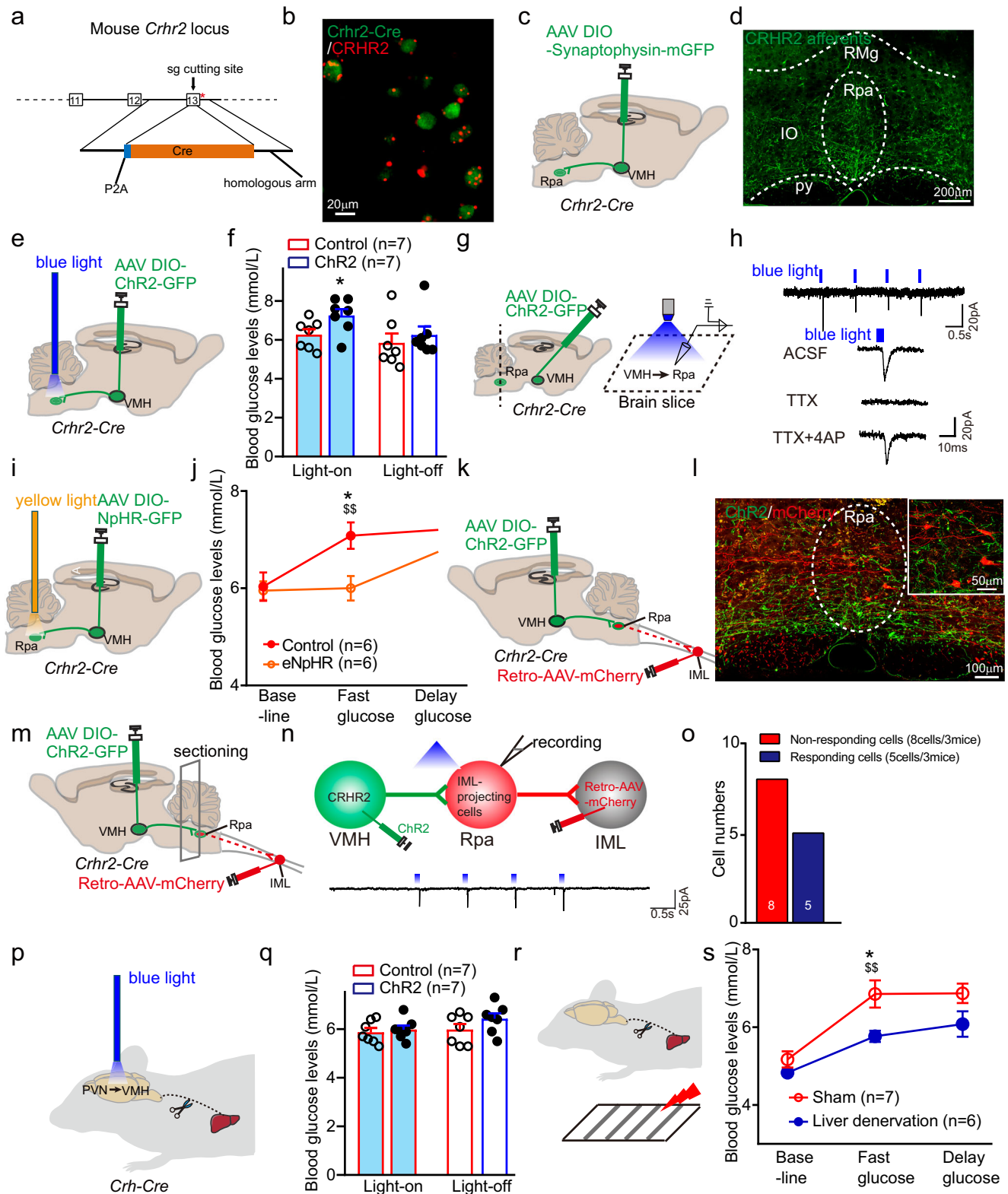
induced a significant decrease of $\beta 3$ GABA_A receptor subunit membrane expression when compared to vehicle group (repeat measurement, group effect $p < 0.001$). $n = 12/3$, cells/repeats. **j** GFP-immunoprecipitation (IP) shows increased S408/409 phosphorylation of $\beta 3$ GABA_A receptors after CRH treatment. The samples derive from the same experiment and the gels/blots were processed in parallel. **k** Statistic for blotting results showed that CRH treatment significantly increased $\beta 3$ receptor at S408/409. $p = 0.012$, $n = 3$ replicates. **l** Schematic of infusion of GABA_A receptor antagonist bicuculline in the VMH. **m** When compared with vehicle group, the administration of bicuculline increased blood glucose levels. $p = 0.006$. Two-sided paired t test in (b, e, g) or unpaired t test in (k, m), two-way repeated-measures ANOVA in (i). All data shown as means \pm SEM. * $p < 0.05$, ** $p < 0.01$, *** $p < 0.001$; ns, not significant. Source data are provided as a Source Data file.

Hypothalamic CRH signal regulates rapid glucose release via the HSL axis activity

Our previous study showed that VMH can control glucose metabolism through the sympathetic pathway¹⁹. We hypothesized that VMH^{CRHR2} regulates stress-induced glucose release can be mediated by sympathetic afferent to the liver. To test this hypothesis, we constructed *Crhr2-Cre* mice using the CRISPR-Cas9 system. Briefly, we replaced exon 13 of *Crhr2* by adding a P2A-Cre homologous arm (Fig. 6a). By injecting Cre-dependent AAV-DIO-EGFP virus, we were able to label CRHR2-positive neurons in the VMH, which were completely colocalized with the *Crhr2* mRNA probe (Fig. 6b), indicating that the Cre recombinases are expressed specifically in CRHR2 neurons.

We next asked whether CRHR2-positive cells send projections to the brain stem to mediate autonomic nervous activity. First, we injected an anterograde tracer, AAV-DIO-Synaptophysin-mGFP, into the VMH of *Crhr2-Cre* mice (Fig. 6c, Supplementary Fig. 7a). Dense labeled terminals were found in brain stem regions, including, dorsal

motor nucleus of the vagus nerve (DMV), and raphe pallidus nucleus (Rpa) and few fibers were found in the nucleus tractus solitarius (NTS) (Fig. 6d, Supplementary Fig. 7b). We further examined these projections using optogenetic activation by injecting AAV-DIO-ChR2-GFP into the VMH region of *Crhr2-Cre* mice. Although VMH^{CRHR2} afferents were found in the DMV and NTS regions, which may mediate activation of parasympathetic nerves, optical stimulation of the VMH^{CRHR2}-DMV/NTS circuit did not affect blood glucose levels (Supplementary Fig. 7c–e). While optical stimulation of VMH^{CRHR2} to Rpa pathway significantly increased blood glucose (Fig. 6e, f, Supplementary Fig. 7f, g). To test whether VMH^{CRHR2} formed monosynaptic connections with Rpa neurons, we expressed AAV-DIO-ChR2 in the CRHR2 neurons. When exposed to blue light, time-locked post-synaptic excitatory currents were found in Rpa neurons, which can be blocked by pre-synaptic blocker TTX and recovered by TTX + 4-AP, indicating a monosynaptic connection between VMH^{CRHR2} and Rpa neurons (Fig. 6g, h). We next investigated whether the VMH^{CRHR2} to Rpa neural circuit is necessary to



mediate stress-induced glucose levels, we injected AAV-DIO-eNpHR-GFP into the VMH of *Crhr2-Cre* mice (Fig. 6i, Supplementary Fig. 7h). As expected, footshock induced an increase in blood glucose levels in the control group, which expressed AAV-DIO-GFP in the VMH.

Optogenetic inhibition of the VMH^{CRHR2} to Rpa blocked the footshock-induced hyperglycemia for fast glucose, but not for delay glucose (Fig. 6j), suggesting that VMH to Rpa projection is necessary to control fast glucose response during stress.

Previous studies have shown that the Rpa receives hypothalamic projections and regulates energy metabolism through the sympathetic nervous system^{25,26}. This pathway is likely mediated by stimulation of intermediolateral nucleus (IML) because hypothalamic neurons promote hepatic glucose production by stimulating IML-mediated sympathetic nervous activity²⁷. Thus, we hypothesized that the CRH signal in VMH-induced hyperglycemia can be mediated by activation of the VMH^{CRHR2}-Rpa-IML connection. To do so, we injected Cre-dependent

Fig. 6 | A descending control of VMH-sympathetic nerve-liver activity mediates CRH effect on stress glucose in VMH. **a** Strategy for design of *Crhr2-Cre* mice by using CRISPR-Cas9 system. **b** Representative image of EGFP co-localization with *Crhr2* mRNA in the VMH. **c, d** Schematic of anterograde tracing virus injection (**c**) and representative image showing CRHR2⁺ afferents in Rpa (**d**). **e** Paradigm for photo-stimulation of CRHR2 terminals in the Rpa. **f** Glucose levels increased after light stimulation of VMH^{CRHR2}→Rpa, **p* = 0.043, control (*n* = 7) vs ChR2 (*n* = 7). **g** Schematic of photo-stimulation of VMH^{CRHR2}→Rpa in brain slices. **h** Example traces for light-evoked time-locked EPSC in the Rpa neurons. **i** Paradigm for photo-inhibition of VMH^{CRHR2}→Rpa during footshock. **j** Footshock-induced increases in fast glucose levels in the control group (\$\$*p* = 0.002), which is blunt by photo-inhibition of CRHR2 terminal in the Rpa (**p* = 0.015), *n* = 6 per group. **k** Paradigm for tracing of VMH^{CRHR2}→Rpa→IML. **l** Representative image showing IML-projecting neurons (red) in Rpa, which is surrounded by CRHR2⁺ afferents (green) from VMH.

AAV-DIO-ChR2-GFP and retro-AAV-mCherry into the VMH and IML, respectively, of *Crhr2-Cre* transgenic mice. IML-projecting cells were found in the Rpa, which is surrounded by ChR2 fibers (Fig. 6k, l), indicating a possible synaptic connection between VMH^{CRHR2} and IML-projecting Rpa neurons. To further confirm our hypothesis, we performed brain stem brain slice recordings by photostimulating the CRHR2⁺ neuronal terminal in the Rpa (Fig. 6m). We found that blue light-evoked EPSCs were detected in IML-projecting Rpa neurons (Fig. 6n, o), suggesting that VMH CRHR2⁺ neurons formed excitatory synapses with IML-projecting cells within the Rpa.

Considering the liver is the main source of endogenous glucose production, we next investigated whether the sympathetic innervation of liver is necessary to mediate CRH's effect on glucose levels. To do so, we utilized phenol-based hepatic sympathetic nerve denervation to reduce the sympathetic nerve activity of the liver as previously described²⁸. Indeed, denervation reduced liver norepinephrine (NE) level about 50% (Supplementary Fig. 8a, b). Consistently, TH fluorescence intensity density was significantly decreased in the liver when comparing with sham group (Supplementary Fig. 8c, d), but not in the pancreas and colon, indicating the denervation was successful in the liver (Supplementary Fig. 8e, f). As we showed in Fig. 2n, opto-stimulation of PVN^{CRH} to VMH increased blood glucose, while this effect was diminished by blunt of sympathetic nerve of liver (Fig. 6p, q). It suggested sympathetic activation is necessary for CRH regulation on glucose levels. Next, we asked whether blunt of hepatic sympathetic nerve should affect fast glucose levels during stress if VMH CRH signal effect on stress-induced fast glucose response is indeed mediated by sympathetic activity. When compared to the sham group, the denervation caused significantly decrease on fast glucose levels post footshock stress (Fig. 6r, s), but not for the delayed glucose response. It suggested that sympathetic nerve activity is required for rapid glucose release during acute stress. Previous studies suggest liver sympathetic regulation of glucose output may involve gluconeogenesis^{2,19}. To investigate whether gluconeogenesis is involved in the HSL axis-mediated glucose release, we measured the activity of key enzymes involved in liver gluconeogenesis. After footshock stress, the mice were immediately sacrificed, and harvest the liver for enzyme activity measurements. Two key enzymes are involved in gluconeogenesis: phosphoenolpyruvate carboxykinase (PEPCK) and glucose-6-phosphatase (G6Pc). The activity of both PEPCK and G6Pc were significantly increased after stress, indicating that a liver gluconeogenesis was indeed involved in the HSL axis-mediated fast glucose release during acute stress (Supplementary Fig. 8g–i).

HSL axis-mediated fast glucose release is required for predatory-evoked flight responses

To further confirm the direct connection between hypothalamic CRH signal with liver, we injected AAV-DIO-mCherry in the VMH of *Sf-1-Cre* mice and the trans-synaptic retrograde tracing agent, pseudorabies virus (PRV) into the liver. We found frequent GFP⁺ neurons in the VMH,

m Schematic of identifying the connection between VMH^{CRHR2} neurons and IML-projecting neurons in Rpa. **n** Photo-stimulation evoked synaptic currents in IML-projecting neurons of Rpa (in 100 μM PTX), indicating an excite projection from VMH^{CRHR2} to Rpa^{IML-projecting}. **o** Statistics of total responding cells showing that over 38% IML-projecting neurons received direct projection from VMH^{CRHR2}. **p** Schematic of opto-stimulation of PVN^{CRH}→VMH after liver denervation. **q** Denervation of liver diminished activation of PVN-VMH induced increases on blood glucose levels. **r** Schematic of footshock stress after liver denervation. **s** Stress-induced increase on fast glucose levels in the sham group (\$\$*p* = 0.002, compared to baseline), which can be suppressed by liver denervation, **p* = 0.02, sham (*n* = 7) vs denervation (*n* = 6). Multi-time point data were analyzed by two-way repeated-measures ANOVA with LSD post hoc comparison, otherwise use two-sided *t* test. All data shown as means ± SEM. Source data are provided as a Source Data file.

which colocalized with SF-1 labeled by mCherry (Fig. 7a), suggesting a VMH-liver connection. In the PVN, we also found colocalization of GFP-labeled liver PRV and immunostaining of CRH (Fig. 7b), indicating a PVN^{CRH}-liver projection.

The activation of the sympathetic-adrenal-medullary axis by releasing epinephrine and norepinephrine also results in blood glucose elevation during stress response²⁹. To isolate the possible time window of SAM axis-mediated glucose release, we performed liver denervation and combined CORT108297 infusion to block the activity of HSL and HPA axes, respectively. By doing so, we found stress-induced blood glucose increases between 3–13 min after stress, but not before 5 min and after 15 min when compared with baseline (Supplementary Fig. 8j, k). To further establish the time course of adrenal-dependent and independent glucose release during stress, we continuously monitored the glucose levels after footshock stress. Again, we found that liver denervation blocked stress-induced fast glucose release at *t* = 0, 1 and 2 min, while ADX-blocked glucose increases in the later phase (>3 min). The time course of ADX and liver denervation groups intercrossed at around 3 min after stress, indicating that HSL axis-mediated time window of glucose increase is between 0 and 3 min, the adrenal activity-mediated time window of delay phase is after 3 min (Fig. 7c). Thus, we confirmed that HSL axis activity is required for the early phase (0–3 min) while the adrenal activity is required for later phase (>3 min) glucose release during stress response.

Quick energy supply is crucial for animal survival when facing to potential threats. We next asked whether the CRH signal in the VMH is needed for the predatory cue-evoked flight responses. To test this hypothesis, we injected the CRHR2 antagonist Astressin2B into the VMH (Fig. 7d). In the presence of the expanding looming shadows to mimic an approaching predator, the animals will initiate escape and hide into the nest³⁰. When blocking CRH signal in VMH by administration of Astressin2B locally, we found that the latency fleeing to the nest was increased, while the flight speed was decreased (Fig. 7e–g). It suggested VMH^{CRHR2} is necessary for predatory cue-evoked flight response. If the HSL axis activity is required for rapid glucose release during stress, hepatic denervation should affect the stress response. To test it, we again utilized the phenol-based hepatic sympathetic nerve denervation to reduce the sympathetic nerve activity of liver (Fig. 7h). To be consisted with administration of Astressin2B in VMH, hepatic denervation caused delayed fleeing latency and decreased flight speed (Fig. 7i–k). It indicated that sympathetic activity is indeed required for flight response, which can be due to its function on rapid glucose release during stress.

Discussion

In the present study, we defined a hypothalamus-sympathetic-liver axis which mediates rapid glucose release independent of adrenal activity during the stress response. The stress signal is integrated into the VMH, central control for glucose levels, via CRHR2-mediated

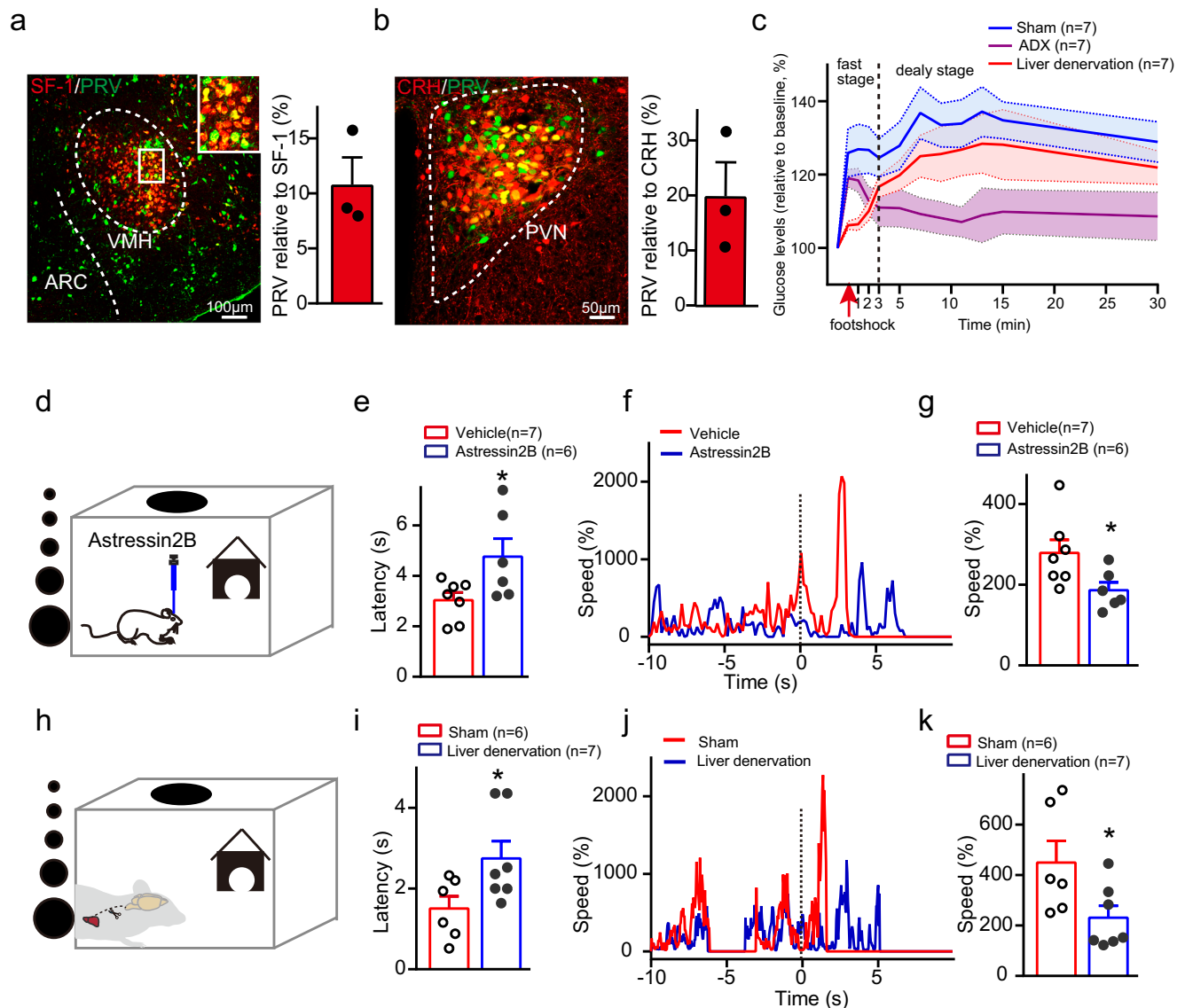


Fig. 7 | HSL axis mediated fast glucose release is required for predatory evoked flight responses. **a** Representative image showing PRV from liver colocalized with SF-1 in the VMH, around 11% SF-1 neurons (red) expressed PRV signal (green). $n = 3$ mice. **b** Representative image showing PRV from liver colocalized with CRH in the PVN, around 20% CRH neurons (red) expressed PRV signal (green). $n = 3$ mice. **c** There is significant difference between the three groups ($p = 0.031$, repeat measurements). Post hoc analysis showed: sham vs denervation group, $p = 0.003$, 0.005 and 0.017 at $t = 0, 1, 2$ min; sham vs ADX group, $p = 0.037$, 0.004 , 0.009 , 0.006 , 0.015 , 0.024 and 0.02 when $t = 5, 7, 9, 11, 13, 15, 30$ min; denervation vs ADX, $p = 0.039$ when $t = 0$ min, $n = 7$ per group. **d** Experimental paradigm for looming stimulus in a nest-containing open field apparatus with Astressin2B infusion in the VMH. **e** Blocking CRH signal in VMH increased the latency towards the nest. $p = 0.039$, veh ($n = 7$) vs astressin2B ($n = 6$). **f** Representative trace showing instant

speed evoked by looming stimulus in vehicle and Astressin2B administration groups. **g** Blocking CRH signal in VMH caused a decrease in flight speed after looming stimulus when compared to vehicle group. $p = 0.04$, veh ($n = 7$) vs astressin2B ($n = 6$). **h** Experimental paradigm for looming stimulus after liver denervation. **i** Liver denervation caused an increase of the latency and decrease in flight speed. $p = 0.044$, sham ($n = 6$) vs denervation ($n = 7$). **j** Representative trace showing instant speed evoked by looming stimulus in sham and liver denervation groups. **k** Liver denervation caused a decrease in flight speed after looming stimulus when compared to sham group. $p = 0.041$, sham ($n = 6$) vs denervation ($n = 7$). Two-way repeated-measures ANOVA with LSD post hoc comparison in (c) and two-sided unpaired t test in (e, g, i, k). All data shown as means \pm SEM. * $p < 0.05$. Source data are provided as a Source Data file.

suppression of inhibitory tone through β_3 GABA_A receptor membrane recruitment (Fig. 8a, b).

During acute stress, the primary outcome of body reaction is releasing glucose to maintain sufficient energy pool. In nature, quick release of glucose is vital for survival when facing potential threats, such as a predator. Tremendous amounts of studies indicated that the HPA and SAM axes are involved in the stress-induced hyperglycemia^{1,7-9,20,31-33}, yet both of these two pathways mediated hyperglycemia cannot satisfy the time course of fast glucose release, as we showed the time window of SAM and HPA axes from couple

of minutes to half hours. As one of the major components of the HPA axis, corticosterone promotes gluconeogenesis in the liver and central nervous system^{1,2}, which takes ~15 min to mediate corticosterone-dependent regulation of stress-induced hyperglycemia. Norepinephrine processes a slow effect on glucose levels^{34,35}, and epinephrine mediates a relatively quick release of glucose, yet it takes couple of minutes to induce a blood glucose increase by administering epinephrine intravenously⁹⁻¹¹. While, the activity of HSL axis was consistently showed to be required for the fast stage of glucose release within minutes. Thus, we define that the acute stress-induced

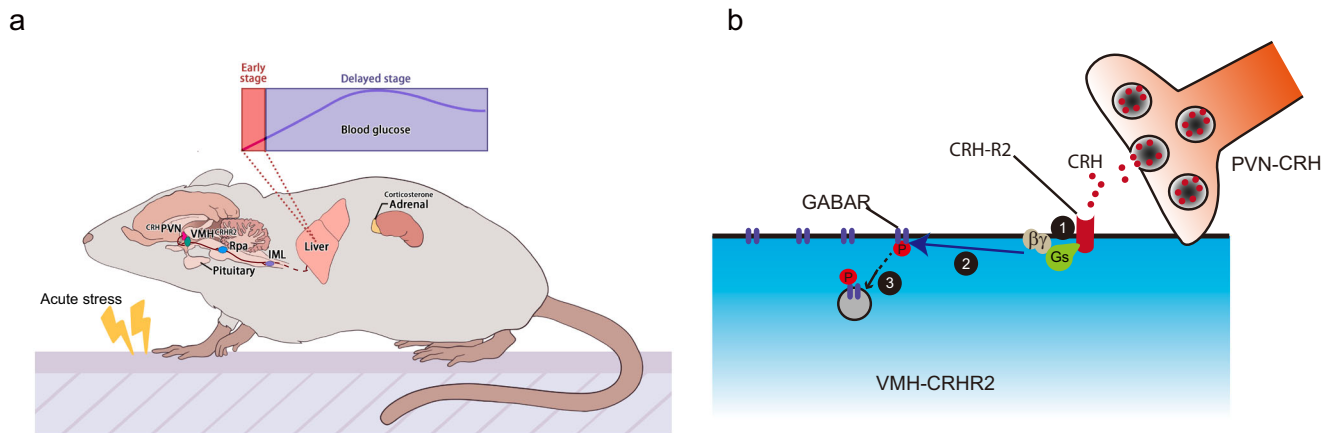


Fig. 8 | Crosstalk between VMH CRH signal and liver mediates rapid glucose release during stress. a The descending controls of PVN^{CRH}-VMH^{CRHR2}-Rpa-IML-liver activity regulate the early stage of stress-induced hyperglycemia in a corticosterone independent manner, while adrenal activation mediates the delayed

stage of glucose release. **b** CRH binding to CRHR2 in VMH increases phosphorylation of S408/409 of $\beta 3$ GABA_A receptor subunit, followed by suppression of GABA_A receptor membrane trafficking, inducing a postsynaptic inhibition of GABAergic tone.

hyperglycemia including at least two different stages: the fast stage (within 3 min), is mediated by HSL axis; the delay stage from 3 to 30 min, is mediated by adrenal activity, including a median stage (within 15 min) mediated by SAM axis and a later stage (after 15 min) mediated by HPA axis.

VMH is a glucose metabolism control center, which triggers counterregulatory hormone release^{16,36}. Interestingly, VMH-SF 1 neurons are also well-known to be implicated in *fight-or-flight* responses and are activated by various acute stressful stimuli including water spray, tail clamp (Supplementary Fig. 2) and predators^{37–39}. Thus, the stress signals are likely integrated in the VMH and further regulates the glucose homeostasis to cope the potential threats. Indeed, when blocking CRH signal in the VMH caused significant impairment of predatory evoked *flight* responses. Our results also showed that different stressors consistently induced fast glucose release, indicating that rapid energy supply is required for all the acute stress responses. Interestingly, blocking the CRH signal in the VMH suppressed this quick glucose response in different stressors, which suggests that the different stressors induced quick glucose release may share the similar pathway mediated by CRH signal in the VMH.

Our previous study showed that endogenous glucose production in the liver can be controlled by VMH neuronal activity through the sympathetic pathway¹⁹. Sympathoexcitatory pathways descending from the hypothalamus must include synapses with premotor neurons at supraspinal levels, which are located within the brain stem⁴⁰. We found that CRHR2-positive cells in the VMH did project to the raphe pallidus, a potential harbor for controlling sympathetic activity. Previous studies have shown that the raphe pallidus receives hypothalamic projections and regulates energy metabolism through the sympathetic nervous system^{25,26,41,42}. Indeed, opto-stimulation of VMH^{CRHR2}-Rpa increased blood glucose while opto-inhibition blocked the fast glucose response during acute stress. Further, if hepatic sympathetic innervation was blunted, the stress-induced fast glucose response was partially diminished. In the liver, two key enzymes are involved in gluconeogenesis: PEPCK and G6Pc. PEPCK is the rate-limiting enzyme required to generate glucose-6-phosphate, whereas G6Pc is the enzyme that cleaves the phosphate allowing for glucose release into the circulation¹. Footshock stress immediately increased both PEPCK and G6Pc activity, suggesting the HSL axis activation induced glucose release is mediated by hepatic gluconeogenesis. Taken together, we provide strong evidence that VMH^{CRHR2} controlled downstream sympathetic flow to regulate early phase of stress-induced hyperglycemia.

Activating CRH receptors induce divergent effects on neural activity dependent on their diverse distribution within the brain¹⁴. For example, activation of CRHR1 in the bed nuclei of the stria terminalis caused the phosphorylation of GluR1 AMPAR subunits, indicating a pre-synaptic function⁴³. Activation of CRHR2 in the central amygdala increased mEPSC amplitude and frequency⁴⁴, indicating both pre-synaptic and postsynaptic function. Acute CRH treatment increases synaptic input and synaptic reliability in mouse CA1 neurons⁴⁵. The VMH is a key central control of energy metabolism^{16,17,19} and receives both excitatory and inhibitory afferents^{46,47}. Our results support that CRH suppresses the inhibitory tone of VMH neurons via a postsynaptic pathway, which is likely mediated by blocking GABA_A receptor membrane trafficking. With respect to GABA_A trafficking, S408/409 phosphorylation in the $\beta 3$ GABA_A receptor subunit has been suggested to be crucial for the recruitment of receptors to the membrane^{23,24}. Although phosphorylation of the $\beta 3$ subunits can mediate both inhibitory and excitatory effects of GABA_A receptors depending on facilitation by the PKA or PKC pathway^{23,24}, the increases in S408/409 phosphorylation mediated the suppressive effect of GABA_A receptor membrane recruitment in the present study. Collectively, we elucidated the CRH-signaling pathway in the VMH, which includes S408/409 phosphorylation in the $\beta 3$ GABA_A receptor subunit, followed by attenuation of GABA_A subunit membrane recruitment and suppression of inhibitory postsynaptic currents, resulting in excitation of VMH neurons.

In summary, we revealed that the stress peptide CRH initiated glucose release composed of rapid and delayed stages, which is regulated by HSL and the adrenal hormones, respectively. The early phase mediated by PVN-VMH-Rpa-sympathetic pathway is necessary to maintain the rapid glucose supply during acute stress—critical for animal survival in event of facing stressors.

Methods

Mice

All experiments involving mice were approved by the Animal Care and Use Committee of the University of Science and Technology of China (USTC) (USTCACUC25120124016). In this study, adult male mice were used at 2–3 months unless otherwise stated. All mice were offered water and food ad libitum, housed (maximum five mice per cage) in a 12 h:12 h light–dark cycle (light from 8:00 A.M. to 8:00 P.M.) with a comfortable temperature (22–25 °C) and 35–55% humidity. For all experiments, mice were randomly allocated into control and treatment groups. WT C57BL/6J, *Crhr1*-flox (#T005812), and *Crhr2*-flox

(#T005813) mice were purchased from GemPharmatech (Nanjing, China). *Crh-Cre* (stock number: 012704), *Ai32* (stock number: 012569), *Sf-1-Cre* (stock number: 012462), and *Crh-Flpo* (stock number: 031559) were purchased from The Jackson Laboratory. *Crh-Cre::Ai32* mice were generated by crossing *Crh-Cre* and *Ai32* genotypes. *Sf-1-Cre::Crh-Flpo* mice were generated by crossing *Sf-1-Cre* and *Crh-Flpo* genotypes. *Sf-1^{Crhr1}-/-* mice were generated by crossing *Crhr1-flox* and *Sf-1-Cre* genotypes. *Sf-1^{Crhr2}-/-* mice were generated by crossing *Crhr2-flox* and *Sf-1-Cre* genotypes. For generating *Crhr2-Cre* mice, the sgRNA targeted the site located at exon #13, and DNA fragments containing homology arms and the 2A-Cre region were constructed. Mixtures of CRHR2-sgRNA (20 ng/μl), Cas9 mRNA (20 ng/μl), and dsDNAs (5 ng/μl) were injected into the nuclei of pronuclear stage mouse embryos. Founders were confirmed by PCR and Sanger sequencing. Genotyping primers for the *Crhr2-Cre* allele were as follows: F1: 5'-GCCATCCCAGACAACCTTAACTT-3'; R1: 5'-TTGGTAAAGGGCTGGTCATCTCT-3'.

Cell culture and transfection

PHluorin-tagged GABA_A receptor subunit γ2 (Gabrg2se, Cat. 49170), and β3 (Gabrb3se, Cat. 49171) plasmids were purchased from Addgene. Untagged GABA_A receptor subunit α1 (Gabra1), γ2 (Gabrg2), and β3 (Gabrb3) were provided as a gift from Dr. Wei Xiong (University of Science and Technology of China). CRHR2 (Cat. 66257) plasmid was purchased from Addgene.

Neuro 2A (N2a, Cat. CCL-131) cell line used for expressing GABA_A receptor subunits and CRHR2 was purchased from ATCC. The N2A cells were cultured using normal DMEM containing 10% fetal bovine serum (Cat. FSP500, Excell Bio) and 1% penicillin/streptomycin solution (Cat. B540732, Sangon, Shanghai, China). Cells were kept in an incubator with 5% CO₂ at 37 °C. Cells were expected to be 70%–90% confluent before transfection. For GABA_A receptor imaging, transfection was performed in 3.5 cm dishes. The ratio of Gabra1, Gabrg2, Gabrb3se, and CRHR2 plasmids was 1:1:1.5. All of the N2a cell transfections were performed using Lipo8000 (Cat. C0533, Beyotime, Shanghai, China). The cells were dissociated with 0.05% trypsin and plated on confocal dishes. Before imaging, the culture medium was replaced with bath solution (144 mM NaCl, 10 mM KCl, 1 mM MgCl₂, 2 mM CaCl₂, 10 mM HEPES, and 10 mM D-glucose, pH 7.4, Osm 315).

Stereotaxic surgery and virus injection

Mice were anesthetized rapidly with 5% isoflurane and then placed on a stereotaxic apparatus (RWD Life Science, Shenzhen, China). During surgery, erythromycin eye ointment was applied to avoid corneal drying, and a heating pad was used to maintain the body temperature. A knife was used to slit the mid-scalp, and a dental drill (B67275, Meisinger, Germany) was used to open a small craniotomy. A 10 μl microsyringe (701 N, HAMILTON, USA) with a calibrated glass micro-electrode (IB 100-3, WPI, USA) was used to inject the virus at a speed of 40 nl/min under a microsyringe pump (UMP3, WPI, USA). After each injection, the microelectrode was left in the site for approximately 5 minutes and moved slowly to minimize virus leakage. Unless otherwise stated, all viruses used in this article were purchased from BrainVTA (Wuhan, China).

For PVN^{CRH} anterograde tracing, 100 nl of AAV-hSyn-DIO-Synaptophysin-mGFP was delivered bilaterally to the PVN (A/P, −0.78 mm from the bregma; M/L, ± 0.26 mm from the midline; D/V, −4.57 mm from the dura) of *Crh-Cre* mice. For VMH^{CRHR2} anterograde tracing, 100 nl of AAV-hSyn-DIO-Synaptophysin-mGFP was delivered bilaterally to the VMH (A/P, −1.46 mm from the bregma; M/L, ±0.45 mm from the midline; D/V, −5.25 mm from the dura) of *Crhr2-Cre* mice.

To study the specific projection from PVN^{CRH} neurons to VMH^{SF-1} neurons, we used a modified rabies virus SAD^G-EGFP(RV-EnvA-ΔG-EGFP) in combination with Cre-dependent helper AAVs expressing TVA (receptor for the avian sarcoma leucosis virus envelope protein EnvA; AAV-ef1α-DIO-mCherry-F2A-TVA) and RG (rabies envelope

glycoprotein; AAV-ef1α-DIO-RVG). *Sf-1-Cre::Crh-Flpo* double transgenic mice were used in this experiment. AAV-DIO-TVA-mCherry and AAV-DIO-RVG (each 100 nl) were injected into the VMH, allowing rabies infection of SF-1 neurons and subsequent retrograde transmonosynaptic spread. At the same time, the Flpo-dependent mCherry (AAV-ef1α-fDIO-mCherry) (Taitool Bioscience, Shanghai, China) virus was injected into the PVN to label CRH-expressing neurons. Three weeks post-AAV transduction, we injected SAD^G-EGFP into the VMH.

For chemogenetic manipulation of CRH neurons in the PVN, 200 nl of AAV-hSyn-DIO-hM₃Dq-mCherry (Taitool Bioscience, Shanghai, China) or AAV-hSyn-DIO-mCherry was delivered bilaterally to the PVN of *Crh-Cre* mice.

For optogenetic manipulation of CRH neurons in the PVN, 200 nl of AAV-ef1α-DIO-ChR2 (H134R)-EGFP/ AAV-ef1α-DIO-eNphR3.0-EGFP were delivered bilaterally to the PVN of *Crh-Cre* mice, and optical fibers were implanted bilaterally in the PVN region.

To activate PVN^{CRH} neuron axon terminals in the VMH, optical fibers were implanted bilaterally in the VMH region of *Crh-Cre::Ai32* mice. To inhibit PVN^{CRH} neuron axon terminals in the VMH, 200 nl of AAV-ef1α-DIO-eNphR3.0-EGFP was first delivered bilaterally to the PVN of *Crh-Cre* mice, and then optic fibers were implanted bilaterally in the VMH region.

To activate VMH^{CRHR2} neuron axon terminals in the Rpa, 100 nl of AAV-ef1α-DIO-ChR2 (H134R)-EGFP was delivered bilaterally to the VMH of *Crhr2-Cre* mice, and an optical fiber was implanted in the Rpa region (A/P, −6.15 mm from the bregma; M/L, ±0.00 mm from the midline; D/V, −4.85 mm from the dura).

To confirm synaptic connection between VMH^{CRHR2} and IML-projection Rpa neurons, 100 nl of AAV-ef1α-DIO-ChR2 (H134R)-EGFP was delivered bilaterally to the VMH of *Crhr2-Cre* mice, and AAV2-hsyn-retro-mcherry was injected into IML (AP, T8-T11 of spinal cord; ML, ±0.35 mm; DV, −0.5 mm).

To record the response of SF-1 neurons to stress, 200 nl of AAV-ef1α-DIO-Gcamp6 was unilaterally injected into the VMH of *Sf-1-Cre* mice, and optic fibers were implanted unilaterally in the same region.

For pharmacological studies, bilateral guide cannulas (outside diameter 0.48 mm, RWD, Shenzhen, China) were implanted in the VMH of *C57/BL6J* mice.

The accuracy of the virus injection site, optic fiber or cannula implantation position were examined on the brain slices post sacrifice. Only the mice with accurate sites were used for statistical analysis.

Adrenalectomy

Mice were deeply anesthetized with sodium pentobarbital (80 mg/kg, i.p.). A 1.5–2 cm dorsal midline incision was made, and the muscles on both sides were incised longitudinally. Then, a curved forceps was used to remove the adrenal glands bilaterally. Postsurgery, mice were placed on a heating pad to recover before returning to their home cages and were supplied with drinking water containing 30 mg/kg ibuprofen for seven days with 0.9% sodium chloride ad libitum. Sham-operated mice underwent the same procedure except that the adrenal glands were not removed. Mice were allowed to recover two weeks from the surgery before starting experiments.

Hepatic sympathetic nerve denervation

After an abdominal midline incision, the hepatic ligaments were loosened, and the portal vein, common duct, and hepatic artery were dissected. A 10% phenol–ethanol solution was applied to these structures with small cotton swabs. Attention was taken to wash the abdominal cavity with saline after the denervation to remove excess phenol and to prevent adhesions. Sham-operated animals were submitted to the same surgical procedures, with the application of 0.9% NaCl solution onto the structures, in substitution for phenol. Postsurgery, mice were placed on a heating pad to recover before returning

to their home cages. Mice were allowed to recover 1 weeks from the surgery before starting experiments.

Immunohistochemistry

The mice were transcardially perfused with 0.9% saline followed by 4% paraformaldehyde in 0.01 M phosphate-buffered saline (PBS), pH 7.4. The brain, liver, pancreas, and colon were collected and postfixed with 4% paraformaldehyde overnight at 4 °C and then transferred into 30% sucrose. Coronal brain slices (40 µm), liver slices (30 µm), gut slices (30 µm) or pancreas slices (30 µm) were prepared by a freezing cryostat (CM1860, Leica). For immunostaining, the sections were washed 3 × 10 min with PBS. Blocking buffer contained 5% donkey serum and 0.4% Triton X-100 in PBS. Sections were then incubated in primary antibodies with 5% donkey serum dissolved in PBS containing 0.4% Triton X-100 overnight for 24 hours at 4 °C. The primary antibody was rabbit anti-c-Fos (1:1000; Cat. sc-52, Santa Cruz), rabbit anti-Tyrosine Hydroxylase (TH) (1:1000; Cat. AB152, Millipore), or rabbit anti-CRH (1:2000; Cat. T4037, Peninsula Laboratories). Next, sections were washed 3 × 5 min with PBS and incubated with secondary antibodies for 12 hours at 4 °C in the dark. The secondary antibody was Alexa Fluor 488-conjugated donkey anti-rabbit (1:500; Cat. 711-545-152, Jackson ImmunoResearch) or Alexa Fluor 594-conjugated donkey anti-rabbit (1:500; Cat. 711-585-152, Jackson ImmunoResearch). Finally, sections were washed 3 × 5 min with PBS followed by mounting on slides with 80% glycerol solution. Immunofluorescence images were captured by using a Zeiss LSM980 confocal microscope (Germany).

Blood sample measurements

All the animals were handled for 5 days before experiments. For chemogenetic experiments, the mice were intraperitoneally injected with 0.9% saline for 3 days adaption to avoid the possible stress during experiments. For optogenetic and cannula experiments, the fibers and infusion needles were connected to the head of mice for additional 3 days adaption to avoid the possible stress during experiments. To measure the blood glucose, a small incision of tail-tip was cut by a surgical blade, and a small drop of blood (<5 µl) was placed on the test strip of the blood glucometer (Abbott, FreeStyle Freedom Lite). For corticosterone measurements, mice were anesthetized rapidly with 5% isoflurane and about 100 µl retro-orbital blood samples were collected into EGTA-coated tubes. The blood samples were centrifuged for 15 min at 1520 × g at 4 °C and serum samples were stored at −80 °C. Each mouse received orbital blood only once per time point. Enzyme-linked immunoassay kits were used to measure serum levels of corticosterone (Cat. D721183, BBI-life sciences).

Co-IP and Western blotting

To purify the pHluorin-tagged GABA_A receptor subunit, a GFP-Trap (Cat. 210611, Chromotek) was used. Briefly, cells were pretreated with either vehicle (PBS) or CRH (100 nM) at 37 °C for 10 min. Then, the cells were collected and solubilized in lysis buffer (10 mM Tris-HCl, 150 mM NaCl, 0.5 mM EDTA, 0.5% NP40, and protease/phosphatase inhibitors) for 30 min at 4 °C. Next, the insoluble fractions were removed by centrifugation at 17,000 × g for 30 min. Then, 40 µl GFP-Trap beads were added to the samples and rotated overnight at 4 °C. Then, the beads were washed five times with wash buffer (10 mM Tris-HCl, 150 mM NaCl, 0.5 mM EDTA, 0.05% NP40, and protease inhibitors), boiled in SDS sample buffer, and subjected to sodium dodecyl sulfate–polyacrylamide gel electrophoresis (SDS–PAGE). Monoclonal antibodies against GFP-tag (Cat. ab183734, Abcam) and polyclonal antibodies against GABA_A receptor β3 Ser408/409 (GTX82680; GeneTex) were used in this study.

Enzyme activity assay

Briefly, the liver (0.1 g) were immediately isolated from mice after footshock and homogenized in 1 ml extraction buffer using tissue homogenizer (JXFSTRP-24, Shanghai Jingxin). Then the homogenates

were centrifuged at 4 °C and 12,000 × g for 10 min, the supernatants were collected and kept at 4 °C. The activity of PEPCK and G6Pc was then determined by the PEPCK activity assay kit (KTBI126, Abbkine) and G6Pc activity assay kit (KTBI014, Abbkine). Enzyme activity was determined using continuous microplate readers (SpectraMax iD5) at 37 °C. The total protein concentration was measured by the BCA protein assay kit (PK10026, Proteintech).

Behavior experiments

Optogenetic experiments. The optogenetic manipulation experiments were performed three to four weeks after viral expression. All the animals were handled for 5 days before experiments, and the fibers were connected to the heads of mice for an additional 3 days of adaption to avoid possible stress during experiments. Optical fibers (1.25 OD zirconium ferrule, 200 µm fiber core, NA = 0.22; (Newdoon, Hangzhou, China) were connected to a rotary joint fiber patch cable (Newdoon, Hangzhou, China) by a mating sleeve (Newdoon, Hangzhou, China). For optogenetic activation, the patch cable was connected to a 473 nm laser, and a stimulator (Master-8) was used to generate blue light pulses (4 ms pulse duration, 20 Hz frequency, 10 min on and 5 min off; 2–5 mw continuous output power measured at 0.2 mm from the fiber tip). For optogenetic inhibition, the patch cable was connected to a 589 nm laser, the 589 nm yellow light was administered for 30 min continuously, and 5–8 mw continuous output power was measured at 0.2 mm from the fiber tip. The mice were subjected to footshock (0.5 mA, 2 s duration with a 6 s interval, for 3 min) stress treatments, and fasting blood glucose was monitored at baseline, immediately after stress, and 30 min after footshock. The mice were fasted for 12 hours before the experiment, and no food was provided during the blood glucose measurement period. To measure the fasting blood glucose, a small drop of tail-tip blood (<5 µl) was placed on the test strip of the blood glucometer (Abbott, FreeStyle Freedom Lite).

DREADD experiment

The chemogenetic manipulation experiments were performed three weeks after viral expression. All the animals were handled for 5 days before experiments and the mice were intraperitoneally injected with 0.9% saline for 3 days adaption to avoid the possible stress during experiments. CNO (Cat. HY-17366, MedChemExpress) was dissolved in dimethylsulfoxide (DMSO, 60 mg/ml) as a stock solution and diluted in 0.9% saline. The fasting glucose levels were measured 30 min after the intraperitoneal injection of CNO (1 mg/kg bodyweight in saline, i.p.).

Fiber-photometry recording

The experiments were performed three weeks after viral expression. All the animals were handled for 5 days before experiments and the fibers were connected to the head of mice for additional 3 days adaption to avoid the possible stress during experiments. Optical fibers (1.25 OD zirconium ferrule, 200 µm fiber core, NA = 0.37; Newdoon, Hangzhou, China) were connected to a rotary joint fiber patch cable (ThinkerTech, Nanjing, China) by a mating sleeve (Newdoon, Hangzhou, China). The patch cable was connected to a fiber-photometry setup (ThinkerTech, Nanjing, China). The emission light was generated by a 480 nm LED, reflected with a dichroic mirror, and delivered to the brain to excite GCaMP6. The emission light was passed through another bandpass filter into a CMOS (complementary metal-oxide semiconductor) detector (Thorlabs Inc.; DCC3240M) and finally recorded by a LabVIEW program (TDMSViewer, ThinkerTech). Mice were recorded for 10 min, and water spray, footshock or tail clips were produced at 5, 6 and 7 min, respectively.

Fiber-photometry signals were processed with custom-written MATLAB software, which is available at <https://zenodo.org/record/6456623#>. YlaF_8hByUk (Zenodo ID: 6456623; Zenodo <https://doi.org/10.5281/zenodo.6456623>; ThinkerTech Nanjing Bioscience, 2020). Data are presented as the relative change in fluorescence ($\Delta F/F$).

Cannula infusion

The experiments were performed one week after surgery. All the animals were handled for 5 days before experiments and infusion needles were connected to the head of mice for additional 3 days adaption to avoid the possible stress during experiments. To block CRH signaling in the VMH, PBS (1 μ l) or Astresssin (3.3 ng in 1 μ l PBS; Cat. HY-P0257, MedChemExpress) was injected into the VMH, and the mice were subjected to footshock (0.5 mA, 2-s duration with a 6-s interval, for 3 min) stress treatment. The fasting blood glucose was monitored at baseline, immediately after stress and 30 min after footshock.

To investigate the different roles of CRHR1 or CRHR2 in regulating stress-induced hyperglycemia, we injected either vehicle (1 μ l of PBS), Astresssin 2B (3.3 ng in 1 μ l PBS; Cat. 2391, Tocris), or R121919 (10 nM in 1 μ l PBS; Cat. HY-14127, MedChemExpress) into the VMH using a guide cannula, and the mice were subjected to footshock (0.5 mA, 2 s duration with a 6 s interval for 3 min) stress treatment. The fasting blood glucose was monitored at baseline, immediately after stress and 30 min after footshock.

Systemic blockade of glucocorticoid receptor (GR)

To block the possible corticosterone effect through its receptor-GR, mifepristone (RU486; Cat. HY-13683, MedChemExpress) was administered intraperitoneally 30 min before each footshock session at a dose of 20 mg/kg. Furthermore, the selective GR antagonist CORT108297 (30 mg/kg; T15000, TargetMol) was administered intraperitoneally 60 min before each footshock session.

Looming test

The looming test was performed in a closed box (40 \times 40 \times 30 cm) with a shelter in the corner. For looming stimulation, an LCD monitor was placed on the ceiling to present multiple looming stimuli, which was a black disc expanding from a visual angle of 2° to 20° in 0.5 s. The expanding disc stimulus was repeated for 20 times in quick succession and this together with a 0.066 s pause between each repeat. Mice were habituated for 10–15 min in the looming box one day before testing. During the looming test, mice were first allowed to freely explore for 3–5 min. We have presented all speeds in relative percentage form compared with baseline average speed. “Baseline” was defined as the period 50 s before onset of the looming stimulation. The average speed during the baseline period was set as 100%.

Electrophysiology

Briefly, animals were anesthetized using isoflurane and euthanized via decapitation. The brain was quickly removed to an ice-cold dissection solution (in mM, 125 NaCl, 2.5 KCl, 1.25 NaH₂PO₄, 25 NaHCO₃, 2.5 D-Glucose, 50 Sucrose, 0.625 CaCl₂, 1.2 MgCl₂, pH 7.3–7.4). Coronal slices were cut in ice-cold dissection solution on a vibrating blade microtome (Cat. VT-1200s, Leica). Slices were maintained for 1 hour at room temperature in artificial cerebrospinal fluid (ACSF, in mM, 125 NaCl, 2.5 KCl, 1.25 NaH₂PO₄, 25 NaHCO₃, 2.5 D-Glucose, 22.5 Sucrose, 2.5 CaCl₂, 1.2 MgCl₂, pH 7.3–7.4). Patch pipettes (5–7 M Ω) were pulled from borosilicate glass and filled with internal solution (in mM, 40 CsCl, 90 K-glucuronate, 10 HEPES, 0.05 EGTA, 1.8 NaCl, 3.5 KCl, 1.7 MgCl₂, 2 Mg-ATP, 0.4 Na₄-GTP, 10 Phosphocreatine and additional 5 mM QX-314 for evoked IPSCs). The ACSF and dissection solution were bubbled with 95% O₂ and 5% CO₂. The bathing solution was kept at room temperature and constantly exchanged through a perfusion system with a flow rate of ~2 mL/min during the experiment. SF-1 neurons were labeled by a previous injection of AAV-DIO-GFP into the VMH of *Sf-1-Cre* mice. Whole-cell patch-clamp recordings were performed using an Axon 700B amplifier. Data were filtered at 2 kHz, digitized at 10 kHz and collected using Clampex 10.2 (Molecular Devices). Series resistance was compensated to 60–70%, and recordings with series resistances of >20 M Ω were rejected. To record IPSCs, CNQX (10 μ M; Cat. C127, Sigma) was added to block AMPA receptors. TTX (1 μ M; Cat. T-550, Alomone) was added to

block action potentials for mIPSC recording. For evoked IPSC recording, stimuli were delivered to the slice via a concentric bipolar electrode (Cat. CBEBE75, FHC). The data were analyzed using Clampfit 10.2.

Quantification and statistical analysis

Statistical analysis was performed using SPSS Statistics 19.0 (IBM, USA) or Microsoft Excel 2013. Two-way repeated-measures ANOVA with post hoc comparison were used for all time-dependent experiments (group number >2), otherwise use one-way ANOVA. When comparing with the baseline (within group) using two-sided, paired *t* test was used to analyze the significance. The cumulative frequency curve was analyzed by the Kolmogorov–Smirnov test. Outliers are removed by using the “Descriptive Statistics” function of SPSS. Statistical significance was set at *p* < 0.05. All the details of the experiments can be found in the figure legends. All data values are presented as the means \pm SEMs.

Reporting summary

Further information on research design is available in the Nature Portfolio Reporting Summary linked to this article.

Data availability

There are no restrictions on data availability in the manuscript. The data generated in this study are provided in the Source Data file. Source data are provided with this paper.

References

- Magomedova, L. and Cummins, C. L., Glucocorticoids and metabolic control. In: *Metabolic control*, Herzig, S., Editor, Springer International Publishing: Cham, 73–93 (2016).
- Yi, C. X. et al. Glucocorticoid signaling in the arcuate nucleus modulates hepatic insulin sensitivity. *Diabetes* **61**, 339–345 (2012).
- Bernal-Mizrachi, C. et al. An afferent vagal nerve pathway links hepatic PPAR α activation to glucocorticoid-induced insulin resistance and hypertension. *Cell Metab.* **5**, 91–102 (2007).
- Valtat, B. et al. Genetic evidence of the programming of beta cell mass and function by glucocorticoids in mice. *Diabetologia* **54**, 350–359 (2011).
- Opherk, C. et al. Inactivation of the glucocorticoid receptor in hepatocytes leads to fasting hypoglycemia and ameliorates hyperglycemia in streptozotocin-induced diabetes mellitus. *Mol. Endocrinol.* **18**, 1346–1353 (2004).
- Nader, N. et al. AMPK regulates metabolic actions of glucocorticoids by phosphorylating the glucocorticoid receptor through p38 MAPK. *Mol. Endocrinol.* **24**, 1748–1764 (2010).
- Hermans, E. J., Henckens, M. J., Joels, M. & Fernandez, G. Dynamic adaptation of large-scale brain networks in response to acute stressors. *Trends Neurosci.* **37**, 304–314 (2014).
- Kudielka, B. M., Buske-Kirschbaum, A., Hellhammer, D. H. & Kirschbaum, C. HPA axis responses to laboratory psychosocial stress in healthy elderly adults, younger adults, and children: impact of age and gender. *Psychoneuroendocrinology* **29**, 83–98 (2004).
- Leimdorfer, A., Arana, R. & Nack, M. H. Hyperglycemia induced by the action of adrenalectomy on the central nervous system. *Am. J. Physiol.* **150**, 588–595 (1947).
- Vicini, P., Avogaro, A., Spilker, M. E., Gallo, A. & Cobelli, C. Epinephrine effects on insulin-glucose dynamics: the labeled IVGTT two-compartment minimal model approach. *Am. J. Physiol. Endocrinol. Metab.* **283**, E78–E84 (2002).
- Ross, A. P., Darling, J. N. & Parent, M. B. Excess intake of fat and sugar potentiates epinephrine-induced hyperglycemia in male rats. *J. Diabetes Complicat.* **29**, 329–337 (2015).
- Myers, M. G. Jr., Affinati, A. H., Richardson, N. & Schwartz, M. W. Central nervous system regulation of organismal energy and glucose homeostasis. *Nat. Metab.* **3**, 737–750 (2021).

13. Swaab, D. F., Bao, A. M. & Lucassen, P. J. The stress system in the human brain in depression and neurodegeneration. *Ageing Res. Rev.* **4**, 141–194 (2005).
14. Gallagher, J. P., Orozco-Cabal, L. F., Liu, J. & Shinnick-Gallagher, P. Synaptic physiology of central CRH system. *Eur. J. Pharm.* **583**, 215–225 (2008).
15. Steckler, T. & Holsboer, F. Corticotropin-releasing hormone receptor subtypes and emotion. *Biol. Psychiatry* **46**, 1480–1508 (1999).
16. Flak, J. N. et al. Ventromedial hypothalamic nucleus neuronal subset regulates blood glucose independently of insulin. *J. Clin. Invest.* **130**, 2943–2952 (2020).
17. He, Y. et al. Estrogen receptor- α expressing neurons in the ventrolateral VMH regulate glucose balance. *Nat. Commun.* **11**, 2165 (2020).
18. Huang, Z. et al. Glucose-sensing glucagon-like peptide-1 receptor neurons in the dorsomedial hypothalamus regulate glucose metabolism. *Sci. Adv.* **8**, eabn5345 (2022).
19. Liu, J. et al. Intrahypothalamic estradiol regulates glucose metabolism via the sympathetic nervous system in female rats. *Diabetes* **62**, 435–443 (2013).
20. Duclos, M., Timofeeva, E., Michel, C. & Richard, D. Corticosterone-dependent metabolic and neuroendocrine abnormalities in obese Zucker rats in relation to feeding. *Am. J. Physiol. Endocrinol. Metab.* **288**, E254–E266 (2005).
21. Sugimoto, Y., Yamada, J. & Noma, T. Effects of anxiolytics, diazepam and tandospirone, on immobilization stress-induced hyperglycemia in mice. *Life Sci.* **63**, 1221–1226 (1998).
22. Brandon, N., Jovanovic, J. & Moss, S. Multiple roles of protein kinases in the modulation of gamma-aminobutyric acid(A) receptor function and cell surface expression. *Pharm. Ther.* **94**, 113–122 (2002).
23. Jacob, T. C., Moss, S. J. & Jurd, R. GABA(A) receptor trafficking and its role in the dynamic modulation of neuronal inhibition. *Nat. Rev. Neurosci.* **9**, 331–343 (2008).
24. Rudolph, U. & Mohler, H. Analysis of GABAA receptor function and dissection of the pharmacology of benzodiazepines and general anesthetics through mouse genetics. *Annu. Rev. Pharm. Toxicol.* **44**, 475–498 (2004).
25. Cerri, M. et al. The inhibition of neurons in the central nervous pathways for thermoregulatory cold defense induces a suspended animation state in the rat. *J. Neurosci.* **33**, 2984–2993 (2013).
26. Madden, C. J. & Morrison, S. F. Central nervous system circuits that control body temperature. *Neurosci. Lett.* **696**, 225–232 (2019).
27. Picard, A. et al. Fgf15 neurons of the dorsomedial hypothalamus control glucagon secretion and hepatic gluconeogenesis. *Diabetes* **70**, 1443–1457 (2021).
28. Hurr, C., Simonyan, H., Morgan, D. A., Rahmouni, K. & Young, C. N. Liver sympathetic denervation reverses obesity-induced hepatic steatosis. *J. Physiol.* **597**, 4565–4580 (2019).
29. Deussing, J. M. & Chen, A. The corticotropin-releasing factor family: physiology of the stress response. *Physiol. Rev.* **98**, 2225–2286 (2018).
30. Yilmaz, M. & Meister, M. Rapid innate defensive responses of mice to looming visual stimuli. *Curr. Biol.* **23**, 2011–2015 (2013).
31. Bale, T. L. et al. Corticotropin-releasing factor receptor-2-deficient mice display abnormal homeostatic responses to challenges of increased dietary fat and cold. *Endocrinology* **144**, 2580–2587 (2003).
32. Dungan, K. M., Braithwaite, S. S. & Preiser, J. C. Stress hyperglycaemia. *Lancet* **373**, 1798–1807 (2009).
33. Kelly, T. R., Cannon, A. L., Stansberry, K. R., Kimball, M. G. & Lattin, C. R. Changes in hypothalamic-pituitary-adrenal axis function, immunity, and glucose during acute infection in house sparrows (*Passer domesticus*). *Gen. Comp. Endocrinol.* **345**, 114388 (2024).
34. Marangou, A. G. et al. Hormonal effects of norepinephrine on acute glucose disposal in humans: a minimal model analysis. *Metabolism* **37**, 885–891 (1988).
35. Stover, J. F., Sakowitz, O. W., Thomale, U. W., Kroppenstedt, S. N. & Unterberg, A. W. Norepinephrine-induced hyperglycemia does not increase cortical lactate in brain-injured rats. *Intensive Care Med.* **28**, 1491–1497 (2002).
36. Borg, W. P., Sherwin, R. S., During, M. J., Borg, M. A. & Shulman, G. I. Local ventromedial hypothalamus glucopenia triggers counter-regulatory hormone release. *Diabetes* **44**, 180–184 (1995).
37. Kunwar, P. S. et al. Ventromedial hypothalamic neurons control a defensive emotion state. *Elife* **4**, e06633 (2015).
38. Silva, B. A. et al. Independent hypothalamic circuits for social and predator fear. *Nat. Neurosci.* **16**, 1731–1733 (2013).
39. Wang, L., Chen, I. Z. & Lin, D. Y. Collateral pathways from the ventromedial hypothalamus mediate defensive behaviors. *Neuron* **85**, 1344–1358 (2015).
40. Strack, A. M., Sawyer, W. B., Hughes, J. H., Platt, K. B. & Loewy, A. D. A general pattern of CNS innervation of the sympathetic outflow demonstrated by transneuronal pseudorabies viral infections. *Brain Res.* **491**, 156–162 (1989).
41. Madden, C. J., Tupone, D., Cano, G. & Morrison, S. F. α 2 adrenergic receptor-mediated inhibition of thermogenesis. *J. Neurosci.* **33**, 2017–2028 (2013).
42. Morrison, S. F. Central control of body temperature. *F1000Res* **5**, F1000 Faculty Rev-880 (2016).
43. Hu, P. et al. Chronic stress induces maladaptive behaviors by activating corticotropin-releasing hormone signaling in the mouse oval bed nucleus of the stria terminalis. *J. Neurosci.* **40**, 2519–2537 (2020).
44. Liu, J. et al. Corticotropin-releasing factor and Urocortin I modulate excitatory glutamatergic synaptic transmission. *J. Neurosci.* **24**, 4020–4029 (2004).
45. Vandaal, D. et al. Corticotropin-releasing factor induces functional and structural synaptic remodelling in acute stress. *Transl. Psychiatry* **11**, 378 (2021).
46. Yang, F. et al. A GABAergic neural circuit in the ventromedial hypothalamus mediates chronic stress-induced bone loss. *J. Clin. Invest.* **130**, 6539–6554 (2020).
47. Lo, L. et al. Connectional architecture of a mouse hypothalamic circuit node controlling social behavior. *Proc. Natl. Acad. Sci. USA* **116**, 7503–7512 (2019).

Acknowledgements

This work was supported by the National Natural Science Foundation of China (31970950, 91957112 to J.L.; 32300841 to Z.H.; 32271176, 81971264 to W.W.), the Natural Science Foundation of Anhui Province (2308085QC86 to Z.H.), the Fundamental Research Funds for the Central Universities (WK2100000032 to Z.H.), the Postdoctoral Fellowship Program of CPSF (GZC20241649 to L.L.). We thank the Institute of Advanced Technology-Huami Joint Laboratory for Brain-Machine Intelligence at the University of Science and Technology of China for partial support (to J.L.). We thank Professor Andries Kalsbeek and Professor Paul Lucassen from the University of Amsterdam for scientific discussions.

Author contributions

J.L., G.B., Z.Z., and C.Z. designed the experiments and wrote the paper. L.L., Z.H., J.Z., M.W., Y.W., and W.W. conducted the experiments. T.Y. W.X., C.W., F.W. provided materials and experimental equipment.

Competing interests

The authors declare no competing interests.

Additional information

Supplementary information The online version contains supplementary material available at <https://doi.org/10.1038/s41467-024-52815-3>.

Correspondence and requests for materials should be addressed to Ji Liu.

Peer review information *Nature Communications* thanks Qingchun Tong, and the other, anonymous, reviewer(s) for their contribution to the peer review of this work. A peer review file is available.

Reprints and permissions information is available at <http://www.nature.com/reprints>

Publisher's note Springer Nature remains neutral with regard to jurisdictional claims in published maps and institutional affiliations.

Open Access This article is licensed under a Creative Commons Attribution-NonCommercial-NoDerivatives 4.0 International License, which permits any non-commercial use, sharing, distribution and reproduction in any medium or format, as long as you give appropriate credit to the original author(s) and the source, provide a link to the Creative Commons licence, and indicate if you modified the licensed material. You do not have permission under this licence to share adapted material derived from this article or parts of it. The images or other third party material in this article are included in the article's Creative Commons licence, unless indicated otherwise in a credit line to the material. If material is not included in the article's Creative Commons licence and your intended use is not permitted by statutory regulation or exceeds the permitted use, you will need to obtain permission directly from the copyright holder. To view a copy of this licence, visit <http://creativecommons.org/licenses/by-nc-nd/4.0/>.

© The Author(s) 2024